
(1)

# First Principles Investigation of Strongly Correlated Electronic Systems by the MCSCF Cluster Method

(MCSCF クラスター法による第一原理からの強相関電子系の研究)

Mikio Eto

江藤　幹雄

Department of Physics
Faculty of Science
University of Tokyo

July, 1990

Thesis

# First Principles Investigation of Strongly Correlated Electronic Systems by the MCSCF Cluster Method

(MCSCF クラスター法による第一原理からの強相関電子系の研究)


**Mikio Eto**

江藤　幹雄

Department of Physics
Faculty of Science
University of Tokyo


July, 1990

## Acknowledgments

The author would like to express his sincerest gratitude to Professor Hiroshi Kamimura for his continual guidance and encouragement throughout the course of the present work. He is indebted to Dr. S. Kato and Dr. O. Sugino for valuable discussions and for providing the program of the MCSCF method. He wishes to thank Dr. N. Kosugi for helpful discussions and for the Hartree-Fock program package $GSCF3$. He is also pleased to acknowledge fruitful discussions with Professor H. Aoki, Dr. N. Shima, Dr. R. Saito, Dr. S. Tsuneyuki and all the members of the research group under Professor H. Kamimura, Professor M. Tsukada and Professor H. Aoki. He is grateful to Dr. David Y. K. Ko for the critical reading of the manuscripts.

Last but not least, he wishes to thank his parents for many years of encouragements.

This work was partly supported by a Grant-in-Aid from Ministry of Education, Science and Culture of Japan. The numerical calculations were performed on HITAC M-682 and S-820/80 at the Computer Center, University of Tokyo.

# Contents

# Chapter 1

# Introduction

How to treat the correlation effect in many-body systems is one of the most important but difficult problems in the field of solid state physics. Recent intensive theoretical studies on the metal-insulator (MI) transition have revealed that electron-electron interactions have essential importance on the electronic states near the MI transition in doped semiconductors [1,2]. In rare-earth metal compounds electrons behave as heavy fermions in the narrow f-band owing to the strong correlation. This has been vigorously studied lately [3]. Electronic correlation also plays an important role in many other materials, *e.g.* deep impurity levels in semiconductors, microclusters, mesoscopic systems, some low dimensional materials, and so on. The copper oxide compound of the high temperature superconductor, which was discovered in 1986 [4], is a further example of these strongly correlated materials. The discovery has stimulated a lot of people to study strong correlation to elucidate the mechanism of the superconductivity which occurs at unusually high temperature. Particularly, the Hubbard model or some other models have been studied intensively to investigate the electronic structures in the strongly correlated systems, using large computers [5,6].

At the same time, several methods have been developed to predict the electronic states in many kinds of materials from first principles. The most powerful and widely used method among them is the band structure calculation based on the local density functional (LDA) principle which approximates the properties of the ground state as functionals of the local electronic density [7]. Although the band structure calculation is a one-body approximation, a part of the correlation effect is thought to be implicitly included in its effective potential, and it has succeeded in describing the electronic structures in many

weakly correlated systems. However, band structure calculations do not work well in the strongly correlated materials. In fact, according to band structure calculations, undoped compounds of the high temperature superconductors are metallic, though they are actually insulators [8,9,10,11]. For other transition metal oxides, which are antiferromagnetic insulators, band structure calculations predict a very narrow band gap or, sometimes, metallic behavior, in contradiction to the experimental results [12,13]. It seems to be necessary to take into account the correlation effect explicitly to describe the electronic structures in strongly correlated materials.

In the field of quantum chemistry the methods of calculating the electronic states of molecules from first principles have been developed. A number of methods have been proposed to calculate the correlation energy beyond the mean field Hartree-Fock method. In these methods the electron correlation is treated explicitly. One of these advanced methods is the Multi-Configuration Self-Consistent Field (MCSCF) method [14,15]. In this one-electron orbitals are determined including a part of the correlation effect, based on the variational principle. Hence it has the advantage that the electronic structures can be represented by a small number of Slater determinants, even when the correlation effect is large.

We applied for the first time the MCSCF method to problems in the field of solid state physics [16]. On the basis of the method, we have calculated the electronic structures of cluster models from first principles, using which we can investigate some of the bulk properties of strongly correlated materials. Our formalism is as follows.

I. We adopt as a model a certain finite-size cluster which is appropriate to describe the properties of the bulk material.

II. We investigate the electronic structure of the cluster, taking into account the correlation effect explicitly by the MCSCF method.

III. From the results we extract the important features of the electronic states and the properties of the bulk system.

We have applied this formalism to investigate the following two systems, in both of which the electronic correlation is essentially important.



The first system we study is the Anderson-localized state in doped semiconductors. In this system both the randomness and the electron-electron interactions play important roles [1,2]. For this reason the MI transition from the insulator side is exceedingly difficult to treat theoretically, and consequently has been little studied. We study the electronic states in uncompensated Si:P from the intermediate to the critical doping concentration region in chapter 3. To treat both of the characteristic effects we adopt clusters consisting of randomly distributed donors and calculate the MCSCF one-electron orbitals which include the correlation effect as well as the coulomb and exchange interactions. Then we carry out the configuration interaction (CI) calculation, taking the orbitals as a basis set. Based on this new representation, we are able to get, for the first time, a clear cut view of the Anderson localized states near the MI transition. Further, we investigate the properties of the MI transition from the new standpoint of approaching it from the insulator side. By taking an ensemble average over fifty clusters, we calculate the bulk properties; specific heat and spin-susceptibility, and are able to explain the experimental results.

In doped semiconductors the compensation induces remarkable changes in various properties. For example, hopping conduction is greatly influenced by the compensation. The critical exponent of the conductivity at the MI transition is reported to be different between the uncompensated and compensated Si:P, which has not been explained theoretically yet. Some other properties are also changed by the compensation in the intermediate concentration region according to experimental works, while there have been few theoretical works on the effect of the compensation in the Anderson-localization region. To elucidate the difference between the uncompensated and the compensated doped semiconductors, it is necessary to investigate the electronic states from the microscopic point of view. In chapter 4 we study the Anderson-localized states in the compensated Si:P. For this purpose we take the cluster which consists both of donors and of acceptors distributed randomly. By the cluster calculation we make clear the different features between the compensated and uncompensated Si:P from the low to the intermediate concentration region and predict the different behavior of the specific heat.

The second subject we study in the present thesis is the copper oxide compounds of the high temperature superconductors, $La_{2-x}Sr_xCuO_4$ and $Nd_{2-x}Ce_xCuO_4$. Both compounds

are anti-ferromagnetic insulators in the absence of dopants, and superconductivity occurs in the former when holes are doped and in the latter when electrons are doped. The electronic structures of these compounds have not yet been clarified even in the normal state owing to the strong correlation effect. To elucidate the electronic structures in both compounds from first principles, we take clusters of $CuO_6$, $Cu_2O_{11}$ and $CuO_4$, $Cu_2O_7$, respectively. The details of calculations and results are presented in chapter 5. By taking account of the strong correlation effect explicitly by the MCSCF and CI methods, we investigate the anti-ferromagnetic coupling in undoped compounds and the states of doped carriers, and clarify the different features between the hole-doped and the electron-doped superconductors.

The organization of the present thesis is as follows. In chapter 2 we explain how to treat the correlation effect by MCSCF method. The chapters 3 – 5 are devoted to the calculations of the electronic structures of doped semiconductors and copper oxide compounds of the high temperature superconductors. In chapter 6 we give a summary and a discussion.



# Chapter 2

# Treatment of the Correlation Effect

The Hamiltonian of many-body systems can be written as,

$$\begin{aligned} H &= H_1 + H_2 \qquad (2.1) \\ H_1 &= \sum_k [\frac{1}{2}\mathrm{p}_k^2 + V(\mathrm{r}_k)] \\ H_2 &= \sum_{k>l} \frac{1}{|\mathrm{r}_k - \mathrm{r}_l|}, \end{aligned}$$

the summations being over the N electrons. $H_1$ is the one-electron part consisting of the kinetic energy and the one-body potential $V$. The functional form of $V$ depends on the system considered, *e.g.* the attractive force from atomic cores, random site energy *etc.*, while $H_2$ is the two-electron part, which includes the Coulomb interaction between electrons.

In the one-body approximation $H_1$ is diagonalized together with the mean field part of $H_2$. The "Correlation energy" is defined as the difference between the real ground state energy including all the many-body effects and the minimum energy in the range of one-body approximation, that is, the Hartree-Fock energy. To treat strongly correlated systems, we are faced with the following problems.

(1) How to include the correlation energy efficiently,

and

(2) How to represent the many-body state clearly when the correlation effect is taken into account.

## 2.1 The Hartree-Fock, the Heitler-London and the CI methods

We start from the one-electron approximation, the Hartree-Fock (HF) method. This method is based on the variational principle and the MCSCF method is a natural generalization.

We consider the system consisting of even number of electrons, $N = 2n$, for simplicity. As a trial function we take a single Slater determinant,

$$\begin{aligned} \Phi_{HF} &= |\psi_1\alpha\psi_1\beta\psi_2\alpha\psi_2\beta\cdots\psi_n\alpha\psi_n\beta| \\ &= a^\dagger_{1\uparrow}a^\dagger_{1\downarrow}a^\dagger_{2\uparrow}a^\dagger_{2\downarrow}\cdots a^\dagger_{n\uparrow}a^\dagger_{n\downarrow}|0>, \end{aligned} \tag{2.2}$$

where $\alpha$ and $\beta$ are up and down spin functions, and $a^\dagger_{i\sigma}$ is the creation operator of an electron in state $i$ with spin $\sigma$. In minimizing the expectation value of the Hamiltonian (2.1) by the wavefunction (2.2), one-electron orbitals $\{\psi_i,\ i = 1,\cdots,n\}$ in the Slater determinant are determined.

The HF orbitals determined by this procedure have the properties shown below.

(i) In the variation the Coulomb terms

$$< ij|\frac{1}{r}|ij >= \int\int \psi^*_i(\mathbf{r}_1)\psi^*_j(\mathbf{r}_2)\frac{1}{|\mathbf{r}_1-\mathbf{r}_2|}\psi_i(\mathbf{r}_1)\psi_j(\mathbf{r}_2)d\mathbf{r}_1d\mathbf{r}_2, \tag{2.3}$$

and the exchange terms

$$< ij|\frac{1}{r}|ji >= \int\int \psi^*_i(\mathbf{r}_1)\psi^*_j(\mathbf{r}_2)\frac{1}{|\mathbf{r}_1-\mathbf{r}_2|}\psi_j(\mathbf{r}_1)\psi_i(\mathbf{r}_2)d\mathbf{r}_1d\mathbf{r}_2, \tag{2.4}$$

are taken into account in the electron-electron interactions. That is, the one-electron orbitals $\{\psi_i,\ i = 1,\cdots,n\}$ are determined self-consistently in the presence of these mean field terms.

(ii) The energy of the one-electron orbital corresponds to the ionization energy when an electron is carried away from the orbital and the other electrons do not relax (Koopmans' theorem).

We represent the wavefunction of (2.2) by the configuration of the electrons' occupation, as in Fig.2.1.



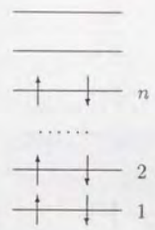


Figure 2.1: The configuration which corresponds to the Hartree-Fock wavefunction (2.2).

Now we go beyond the HF method to describe the correlation effects. We take a hydrogen molecule as the simplest example. There are two methods for solving this molecule. One is the Heitler-London approach which starts from the atomic orbitals, and the other is the molecular orbital approach. (i) In the Heitler-London approach the wavefunction is taken to be

$$\begin{aligned} \Phi_{HL} = &\frac{1}{\sqrt{2(1+S^2)}}[u_A(\mathbf{r}_1)u_B(\mathbf{r}_2) + u_B(\mathbf{r}_1)u_A(\mathbf{r}_2)] \\ &\times\frac{1}{\sqrt{2}}[\alpha(\sigma_1)\beta(\sigma_2) - \beta(\sigma_1)\alpha(\sigma_2)], \end{aligned} \tag{2.5}$$

where $\mathrm{u}_A$ ($\mathrm{u}_B$) is the atomic orbital of a A (B) hydrogen atom and S is the overlap integral of the two orbitals. The wavefunction (2.5) includes the correlation effect since it keeps the electrons from each other. (ii) In the molecular orbital approach we start from the HF wavefunction,

$$\Phi_{HF} = |\psi_+\alpha\psi_+\beta|, \tag{2.6}$$

where the bonding ($\psi_+$) and anti-bonding ($\psi_-$) orbitals are given by

$$\psi_\pm = \frac{1}{\sqrt{2(1\pm S)}}(u_A \pm u_B). \tag{2.7}$$

We can take into account the correlation effect by adding the other Slater-determinant states to (2.6), such as,

$$\Phi_{CI} = C_1|\psi_+\alpha\psi_+\beta| + C_2|\psi_-\alpha\psi_-\beta|. \tag{2.8}$$

The appearance of the other states is due to the many-body interactions and is called the configuration interaction (CI). The coefficients $C_1$ and $C_2$ in (2.8) may be determined by

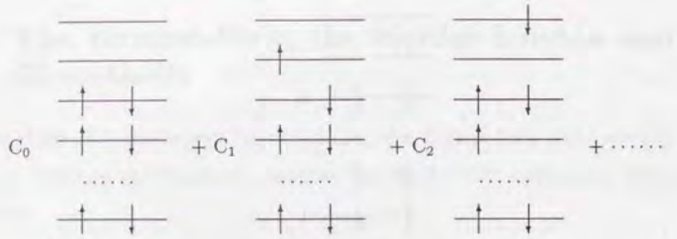


Figure 2.2: The many-body wavefunction of the CI calculation in $2n$-electron system.

minimizing the expectation value of the energy. This CI wavefunction, (2.8), includes the Heitler-London wavefunction (2.5) as the special case of $C_1/C_2 = -(1+S)/(1-S)$.

In an N-electron system we must take the linear combination of many number of configurations, as seen in Fig.2.2, to take account of the correlation effect. We determine the coefficients $\{C_k\}$ of configurations by diagonalizing the Hamiltonian in the configuration space. (In this procedure we can get the excited states as well as the ground state.) Generally, a large number of configurations are necessary to represent the ground state when the correlation effect is strong. Thus we would like to optimize the one-electron orbitals so that we get as large a correlation energy as possible with the smallest number of configurations.

## 2.2 The MCSCF Method

The MCSCF method was developed from the standpoint of obtaining the best one-electron orbitals to be used in the CI calculation [14,15]. A trial function in this method is expressed as a linear combination of several Slater determinants;

$$\begin{aligned} \Phi_{MCSCF} &= \tilde{C}_0\Psi_0 + \sum_i \sum_a \tilde{C}_{ii}^{aa}\Psi_{ii}^{aa} \\ &= (\tilde{C}_0 + \sum_i \sum_a \tilde{C}_{ii}^{aa} a_{a\uparrow}^\dagger a_{a\downarrow}^\dagger a_{i\downarrow} a_{i\uparrow})\Psi_0, \end{aligned} \tag{2.9}$$

where $\Psi_0$ is the same configuration as the HF wavefunction; $|\psi_1\alpha\psi_1\beta\psi_2\alpha\psi_2\beta\cdots\psi_n\alpha\psi_n\beta|$, and the $\Psi_{ii}^{aa}$ 's correspond to the excited configurations in which one spin-up and one spin-down electrons are transferred simultaneously from an occupied $i$ orbital in the configuration $\Psi_0$ into its unoccupied $a$ orbital. In minimizing the expectation value of the



Hamiltonian by this trial function, the one-electron orbitals $\psi_i$'s , $\psi_a$'s, and the CI coefficients $\tilde{C}_{ii}^{aa}$'s in (2.9) are determined simultaneously in the self-consistent way. Then the MCSCF orbitals have the following features:

(i) Not only the Coulomb (2.3) and the exchange energies (2.4) but also the part of the electron correlation represented by the matrix elements,

$$< aa|\frac{1}{r}|ii >= \int\int \psi_a^*(\mathbf{r}_1)\psi_a^*(\mathbf{r}_2)\frac{1}{|\mathbf{r}_1-\mathbf{r}_2|}\psi_i(\mathbf{r}_1)\psi_i(\mathbf{r}_2)d\mathbf{r}_1 d\mathbf{r}_2, \tag{2.10}$$

are taken into account.

(ii) When the CI calculation is carried out using the MCSCF orbitals as a basis set, a small number of configurations is necessary to represent the ground state (MCSCF-CI method). Thus we can get a clear cut view of the many-body state even when the correlation effect is strong.

(iii) Owing to the correlation effect involved, MCSCF one-electron orbitals tend to be localized in a space, compared with the HF orbitals.

The above type of electron-electron interactions (2.10) is the largest besides the mean field HF terms. Physically speaking, the correlation effect is the strongest when two electrons have the opposite direction of spins and are at the same place (or occupy the same orbital). Thus the dominant part of the correlation energy is expected to be included by adopting the trial function (2.9). We may select other trial functions than (2.9), for example, we use a much larger trial function including all kinds of excited configurations in the Complete Active Space Self-Consistent Field (CASSCF) method [17]. But this is not suitable for the purpose of understanding clearly the physics of the electronic states using a small number of CI's.

Although the MCSCF orbitals are suitable to represent strong correlation, each one-electron orbital doesn't have as clear a physical meaning by itself as a HF orbital because electrons do not move independently but are correlated to each other in this case. These orbitals are "effective" one-electron orbitals optimized for the representation of the many-body states in the form of the CI wavefunction.

Thus far we consider the spin-singlet wavefunction. This can be easily extended to the case of spin-triplet. The MCSCF trial function of spin-triplet is shown in Fig.2.3. Here the

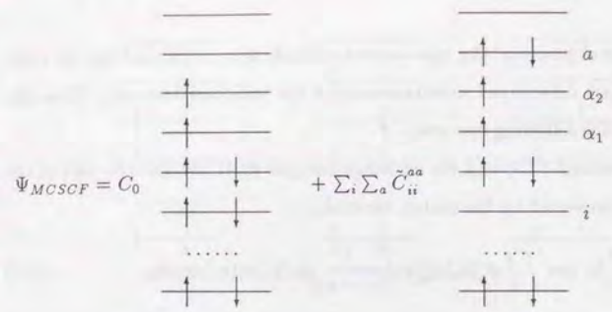


Figure 2.3: The MCSCF trial function for the spin-triplet state.

orbitals $\psi_{\alpha 1}$ and $\psi_{\alpha 2}$ are always singly occupied. Then one-electron orbitals $\psi_i$, $\psi_a$, $\psi_{\alpha 1}$, $\psi_{\alpha 2}$ are optimized in the variation. We adopt this method to obtain the spin-triplet ground state in chapter 5 to determine which of the spin-singlet or the spin-triplet states is stable.

Generally, however, the correlation effect is smaller in the high-spin state because the correlation between electrons of the same spin is included by the Pauli's exclusion principle in the HF approximation already. The rest of the correlation effect can be taken into account in the MCSCF calculation for the spin-singlet state. Hence the MCSCF orbitals optimized for the spin-singlet state may also be used to represent the spin-triplet state. In fact, we can represent the spin-triplet state by a small number of configurations based on the spin-singlet MCSCF orbitals, as will be seen in the next chapter. For this reason we only carry out the MCSCF calculation for the spin-singlet state even for the spin-triplet clusters in chapter 3 and 4. (In these chapters, we perform the full CI calculation and take account of all the electron-electron interactions, and thus the calculated state energies do not depend on the selection of the one-electron orbitals.)



# Chapter 3

# Uncompensated Si:P Systems

## 3.1 Introduction

The electronic structure of doped semiconductors is one of the most interesting topics in condensed matter physics in recent years. In the low concentration region of doped impurities in n-type semiconductors, every dopant electron is localized around a donor, and hopping conduction is observed at low temperatures. As the donor concentration increases, the wavefunction of an electron becomes extended over several donors in the intermediate concentration region, and when the dopant concentration reaches a critical concentration, $n_c$, a metal-insulator (MI) transition takes place.

In the metal-insulator transition of doped semiconductors both disorder and electron-electron interactions play important roles [1,2,18,19]. For some time, intensive theoretical studies have been made to clarify the mechanism of the transition, as well as the nature of the electronic states near the transition. On the metal side of the transition, a number of theoretical works have been made on the precursor behaviors of the transition [20,21], following the appearance of the scaling theory in 1979 [22]. On the insulator side, however, a few theoretical works have been reported, because of the extreme difficulty in treating the strong electron correlation in the neighborhood of the transition.

On the insulator side of the transition, Kamimura and coworkers developed a 'transfer-diagonal' representation formalism to treat both the disorder effect and the electron-electron interactions on an equal footing [23,24]. They first diagonalize the one-electron part of the Hamiltonian (2.1), including the random site energies, and then calculate the effects of the electron-electron interactions by perturbation. By taking into account the intra-state inter-

action, Yamaguchi *et al.* showed that there are singly-occupied states, as well as doubly-occupied and unoccupied states, and succeeded in explaining the observed temperature dependence of the T-linear specific heat and the spin susceptibility in Si:P [25]. Takemori and Kamimura then proposed the "spin pair model" in which each singly-occupied state forms a spin pair with the state which has the largest interstate interaction, and succeeded in explaining the enhancement of the specific heat observed at low temperatures and its magnetic field dependence [26]. In their spin pair model, about half of the spin pairs are spin-singlet. The rest are spin-triplet. Later, Gan and Lee applied the transfer diagonal formalism to explain the temperature and magnetic-field dependence of the relaxation time in NMR experiments [27].

Andres and coworkers also suggested the treatment of magnetic properties by the spin pair approximation in the low concentration region [28]. Later, Bhatt and Lee developed a scaling theory applicable to the higher concentration region below the MI transition, based on the spin pair approximation of randomly localized spin system [29]. In their model all spin-spin interactions are originally anti-ferromagnetic but after the scaling procedure they found that some effective couplings become ferromagnetic for certain spin pairs. Though their approximation is better at low dopant concentrations, the agreement with experiments on spin-susceptibility, magnetization, NMR *etc.*, is good even near the critical concentration at which the MI transition takes place [30,31].

From these considerations, the following questions arise.

(i) How does an electronic state change in the intermediate to the critical concentration regions?

(ii) Why does the spin pair approximation hold even in the neighborhood of the transition?

(iii) How does spin triplet pairing appear?

Computer calculation is the most powerful method to address these questions. From this standpoint, Takemori and Kamimura performed simulation studies on a cluster consisting of six randomly distributed donors, using the basis states of the transfer diagonal formalism [32]. After diagonalizing the effective one-electron Hamiltonian of the clusters, they performed the configuration interaction (CI) calculation with the resulting basis set



to take into account the effects of all the remaining electron-electron interactions. They showed that the formalism works very well in the intermediate concentration region, and that the spin pair model is suitable for the representation of the electronic states there.

However, with increasing donor concentration up to the critical concentration, the formalism faces some difficulties with regards to performing the numerical calculations. In their simulation a considerable number of configurations are necessary to describe the electronic states in the critical region. This indicates physically that the electron-electron interactions are too large to be treated as a perturbation near the MI transition.

To represent the electronic states from the intermediate to the critical concentration region, we have developed a new representation formalism [16]. First, we determine the one-electron orbitals by the MCSCF method, and then calculate the many-body wavefunctions, taking the MCSCF orbitals as a basis set. In this chapter we apply this formalism to the same cluster model as the one Takemori and Kamimura adopted. Since part of the correlation is already included in the MCSCF one-electron orbitals, this new representation formalism is suitable even up to the critical donor concentration region in which the electron correlation is very strong. On the basis of the results obtained, we discuss the mechanism of the metal-insulator transition from a new point of view.

The organization of this chapter is the following. In the next section we explain the cluster model and the simulation formalism. In section 3.3 we give the calculated results in the cluster simulation. We calculate the specific heat and the spin-susceptibility using the results of the cluster calculations. In section 3.4 we present the calculated results and explain the experimental results. Finally, conclusions and discussions are given in section 3.5.

To simulate the system of doped semiconductors, we adopt the effective mass approximation, in which the Hamiltonian can be written as

$$H = \sum_{k=1}^{6} \left( \frac{1}{2} \mathbf{p}_k^2 - \sum_{\nu=1}^{6} \frac{1}{|\mathbf{r}_k - \mathbf{R}_\nu|} \right) + \sum_{k>l} \frac{1}{|\mathbf{r}_k - \mathbf{r}_l|}, \tag{3.1}$$

where $\mathbf{r}_k$ and $\mathbf{p}_k$ are, respectively, the real space coordinate and the momentum of the $k$-th electron, and $\mathbf{R}_\nu$ is the coordinate of the $\nu$-th donor center. Effective atomic units are used throughout unless otherwise stated, in this and the next chapters. The units of length and

energy are 19.63Å and 60.8meV, respectively. The valley degeneracy of the semiconductor is ignored.

## 3.2 Cluster Calculation Method

As a model we adopt a cluster consisting of six donors distributed randomly in a sphere. The radius of the sphere is determined corresponding to the donor concentrations, $N_D$ = (1.0, 1.7, 2.4, 3.2)$\times 10^{18} cm^{-3}$, which correspond to the intermediate to the critical concentration region of Si:P. Then a Gaussian-type hydrogen 1s orbital, $|\nu > \propto \exp(-\lambda|\mathbf{r} - \mathbf{R}_\nu|^2)$ is attached to the $\nu$-th donor atom, in which $\lambda$ is given as $8/9\pi$ by minimization of the binding energy of an isolated donor. By adopting Gaussian orbitals all the matrix elements of Hamiltonian (3.1) can be calculated analytically.

The one-electron orbitals, which are represented by linear combinations of the six Gaussian-type orbitals, are determined by the MCSCF method. In the MCSCF method we consider all pair-type excitations from the lower three orbitals to the upper three orbitals,

$$\begin{aligned} \Phi_{MCSCF} &= \tilde{C}_0\Psi_0 + \sum_{i=1}^{3}\sum_{a=4}^{6}\tilde{C}_{ii}^{aa}\Psi_{ii}^{aa} \\ &= (\tilde{C}_0 + \sum_{i=1}^{3}\sum_{a=4}^{6}\tilde{C}_{ii}^{aa}a_{a\uparrow}^{\dagger}a_{a\downarrow}^{\dagger}a_{i\downarrow}a_{i\uparrow})\Psi_0, \end{aligned} \tag{3.2}$$

where $\Psi_0 = |\psi_1\alpha\psi_1\beta\psi_2\alpha\psi_2\beta\psi_3\alpha\psi_3\beta|$. These one-electron orbitals $\{\psi_k, k = 1, \cdots, 6\}$ form a basis set of our representation.

In the final step of the calculation, the configuration interaction (CI) calculation is carried out using the MCSCF orbitals, and the many-body wavefunctions and their energies are determined. In the CI calculation we include all configurations of 6 electrons occupying 6 orbitals (full CI). We use a free boundary condition for the clusters in the MCSCF and the CI calculations.

Since every many-electron level of a cluster is an eigenstate of total spin, S, and of its z-component, $S_z$, in real numerical calculations it is convenient to confine ourselves to the subspace with $S_z$=0. Then the number of configurations in the CI calculation is reduced to $({}_6C_3)^2 = 400$ from 924, which is the total number of configurations composed of six one-electron orbitals occupied by six electrons.



The calculations are performed for fifty clusters for each impurity concentration.

## 3.3 Calculated Results

The ground state is found to be a spin-singlet in most of the 50 clusters, while 10 % to 20 % of them have the spin-triplet ground state.

The advantage of using MCSCF one-electron orbitals as a basis set is that the CI wavefunctions can be expressed by a small number of configurations. For example, the CI wavefunctions of the ground states of a spin-singlet cluster and a spin-triplet cluster for $N_D = 1.7 \times 10^{18} cm^{-3}$ are shown below.

$$\begin{aligned} \Phi_{Singlet} = {} & 0.75|\psi_1\alpha\psi_1\beta\psi_2\alpha\psi_2\beta\psi_3\alpha\psi_3\beta| - 0.65|\psi_1\alpha\psi_1\beta\psi_2\alpha\psi_2\beta\psi_4\alpha\psi_4\beta| \\ & -0.09|\psi_1\alpha\psi_1\beta\psi_3\alpha\psi_3\beta\psi_5\alpha\psi_5\beta| + 0.08|\psi_1\alpha\psi_1\beta\psi_4\alpha\psi_4\beta\psi_5\alpha\psi_5\beta|, \end{aligned} \tag{3.3}$$

and

$$\begin{aligned} \Phi_{Triplet} = {} & 0.56\{|\psi_1\alpha\psi_1\beta\psi_2\alpha\psi_2\beta\psi_3\alpha\psi_4\beta| + |\psi_1\alpha\psi_1\beta\psi_2\alpha\psi_2\beta\psi_3\beta\psi_4\alpha|\} \\ & +0.30\{|\psi_1\alpha\psi_1\beta\psi_3\alpha\psi_4\beta\psi_5\alpha\psi_5\beta| + |\psi_1\alpha\psi_1\beta\psi_3\beta\psi_4\alpha\psi_5\alpha\psi_5\beta|\} \\ & +0.18\{|\psi_2\alpha\psi_2\beta\psi_3\alpha\psi_4\beta\psi_6\alpha\psi_6\beta| + |\psi_2\alpha\psi_2\beta\psi_3\beta\psi_4\alpha\psi_6\alpha\psi_6\beta|\} \\ & +0.10\{|\psi_3\alpha\psi_4\beta\psi_5\alpha\psi_5\beta\psi_6\alpha\psi_6\beta| + |\psi_3\beta\psi_4\alpha\psi_5\alpha\psi_5\beta\psi_6\alpha\psi_6\beta|\}. \end{aligned} \tag{3.4}$$

For higher dopant concentrations the CI wavefunctions may also be expressed by a small number of configurations only. Thus it is easy to get a clear cut view of the electronic states, even near the MI transition. It is possible, therefore, to discuss the change in the electronic states from the low concentration region to the critical region continuously, as will be seen in the following two example clusters. In this context we may say that the adoption of the MCSCF one-electron orbitals is highly suitable for the representation of the many-body states in this strongly correlated random system.

a) Spin-singlet clusters

One example of the spin-singlet clusters is shown in Fig.3.1. The ground state of the cluster corresponds to the wavefunction (3.3) for $N_D = 1.7 \times 10^{18} cm^{-3}$. For the lowest

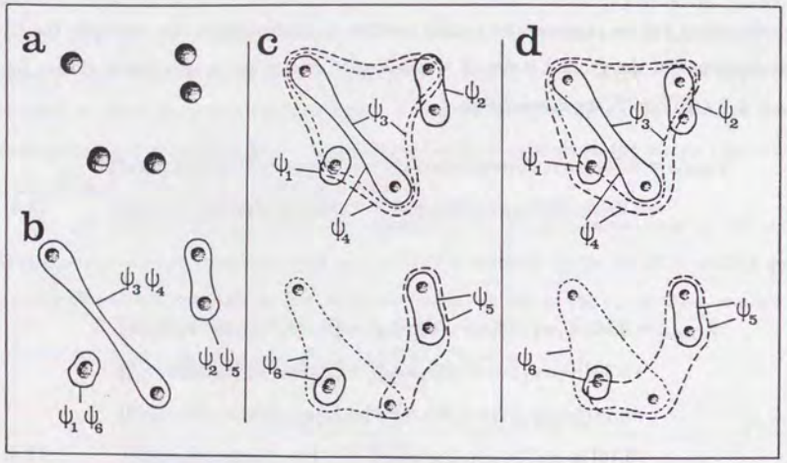


Figure 3.1: An example of the spin-singlet clusters. The geometrical arrangement of six donor atoms (a) and MCSCF one-electron orbitals are shown schematically for the four donor concentrations: $N_D = 1.0 \times 10^{18} cm^{-3}$ (b), $1.7 \times 10^{18} cm^{-3}$ (c), and $2.4 \sim 3.2 \times 10^{18} cm^{-3}$ (d). It should be noted that the two donor atoms at the left bottom corner are very close to each other. In (b),(c) and (d), the solid and broken lines correspond to the highest and the lowest amplitudes of the MCSCF orbitals, respectively.



| $N_D$ ($cm^{-3}$) | Ground state[a] | | | | First excited state[b] | |
|---|---|---|---|---|---|---|
| | $C_0$ | $C_{33}^{44}$ | $C_{22}^{55}$ | $C_{2233}^{4455}$ | $C_3^4$ | $C_{223}^{554}$ |
| $1.0 \times 10^{18}$ | 0.71 | −0.69 | −0.11 | 0.11 | 0.70 | 0.11 |
| $1.7 \times 10^{18}$ | 0.75 | −0.65 | −0.09 | 0.08 | 0.70 | 0.08 |
| $2.4 \times 10^{18}$ | 0.79 | −0.60 | −0.08 | 0.06 | 0.70 | 0.07 |
| $3.2 \times 10^{18}$ | 0.84 | −0.54 | −0.07 | — | 0.70 | 0.06 |

a) $\Phi_g = C_0 |\psi_1\alpha\psi_1\beta\psi_2\alpha\psi_2\beta\psi_3\alpha\psi_3\beta| + C_{33}^{44} |\psi_1\alpha\psi_1\beta\psi_3\alpha\psi_2\beta\psi_4\alpha\psi_4\beta| + C_{22}^{55} |\psi_1\alpha\psi_1\beta\psi_3\alpha\psi_3\beta\psi_5\alpha\psi_5\beta| + C_{2233}^{4455} |\psi_1\alpha\psi_1\beta\psi_4\alpha\psi_4\beta\psi_5\alpha\psi_5\beta|$,

b) $\Phi_{ex} = C_3^4\{|\psi_1\alpha\psi_1\beta\psi_2\alpha\psi_2\beta\psi_3\alpha\psi_4\beta| + |\psi_1\alpha\psi_1\beta\psi_2\alpha\psi_2\beta\psi_3\beta\psi_4\alpha|\} + C_{223}^{554}\{|\psi_1\alpha\psi_1\beta\psi_3\alpha\psi_4\beta\psi_5\alpha\psi_5\beta| + |\psi_1\alpha\psi_1\beta\psi_3\beta\psi_4\alpha\psi_5\alpha\psi_5\beta|\}$.

Table 3.1: Coefficients of the CI wavefunctions of the ground and the first-excited states of the spin-singlet cluster shown in Fig.3.1. All the coefficients larger than 0.05 are listed.

concentration, $N_D = 1.0 \times 10^{18} cm^{-3}$, which is just the border between the low and the intermediate concentration regions, all the MCSCF one-electron orbitals, $\psi_k$, with k=1 to 6, are localized to within two donors. The localized nature of the one-electron orbitals reflects the correlation effect involved in the MCSCF method. For the higher concentrations, $\psi_1$ and $\psi_2$, corresponding to the lower energy states, have almost the same form as those of the lowest concentration and are well localized. The other four MCSCF orbitals become more extended as the concentration increases, although the regions of their highest charge density do not change, as indicated by the solid lines in Fig.3.1.

CI wave functions of the ground state and the first excited state of this spin-singlet cluster are given in Table 3.1 for four donor concentrations. The CI wavefunctions for the above-mentioned four concentrations can be rewritten in a more useful form. For example, those for $N_D = 1.7 \times 10^{18} cm^{-3}$ are shown below;

$$\Phi_{Singlet}^{(g)} = a_{1\uparrow}^\dagger a_{1\downarrow}^\dagger (0.99 a_{2\uparrow}^\dagger a_{2\downarrow}^\dagger - 0.12 a_{5\uparrow}^\dagger a_{5\downarrow}^\dagger)(0.75 a_{3\uparrow}^\dagger a_{3\downarrow}^\dagger - 0.66 a_{4\uparrow}^\dagger a_{4\downarrow}^\dagger)|0>, \quad (3.5)$$

$$\Phi_{Singlet}^{(ex)} = a_{1\uparrow}^\dagger a_{1\downarrow}^\dagger (0.99 a_{2\uparrow}^\dagger a_{2\downarrow}^\dagger - 0.12 a_{5\uparrow}^\dagger a_{5\downarrow}^\dagger) \frac{1}{\sqrt{2}} (a_{3\uparrow}^\dagger a_{4\downarrow}^\dagger - a_{3\downarrow}^\dagger a_{4\uparrow}^\dagger)|0> . \quad (3.6)$$

Let us examine the properties of each MCSCF one-electron orbital, $\psi_k$, corresponding to the creation operator $a_k^\dagger$ in detail. The $\psi_3$ and $\psi_4$ are bonding- and anti-bonding-type orbitals, respectively. Both of them are localized in almost the same region, as have been shown in Fig.3.1. The $\psi_2$ and $\psi_5$ are also respectively bonding- and anti-bonding-type

orbitals between the two donors which are not covered by $\psi_3$ and $\psi_4$. The $\psi_1$ and $\psi_6$ are also in a relation similar to the above. This indicates that the ground state (3.5) can be regarded as consisting of three spin-singlet pairs. Each spin pair is described by a mixture of a configuration in which two electrons occupy a bonding orbital and of another configuration in which two electrons occupy an anti-bonding orbital, just like a Heitler-London wavefunction in a hydrogen molecule. These spin pairs do not interact with each other significantly. On the other hand, in the first excited state (3.6), the two electrons in $\psi_3$ and $\psi_4$ form a spin-triplet pair, while the other spin pairs are the same as those in the ground state (3.5). This is the situation of the spin pair model proposed by Takemori and Kamimura [26]. In higher dopant concentrations, the MCSCF one-electron orbitals are extended, but their bonding and anti-bonding natures are the same in their highest charge density regions. Thus the situation of the spin pair model also holds for the higher dopant concentration region, even though the spin pairs are extended and overlap well with each other.

As for the concentration dependence of the wavefunctions, Table 1 shows that the ground state approaches a single configuration, $|\psi_1\alpha\psi_1\beta\psi_2\alpha\psi_2\beta\psi_3\alpha\psi_3\beta|$, with increasing donor concentration. In each spin-pair, the ratio of the occupation fraction of a bonding-type orbital to that of an anti-bonding orbital increases. This indicates that the electron correlation decreases as the concentration increases to the MI transition.

b) Spin-triplet clusters

Spin-triplet clusters are found to have a common feature, that is, orbitals extended over three donor atoms always appear even for the lowest concentration.

For example, the spin-triplet cluster corresponding to the wavefunction (3.4) is shown in Fig.3.2, where $\psi_3$ is extended over three donors while $\psi_4$ is extended over two donors. The wavefunction of the ground state (3.4) can be factorised as,

$$\Phi^{(g)}_{Triplet} = (0.95a^{\dagger}_{1\uparrow}a^{\dagger}_{1\downarrow} - 0.31a^{\dagger}_{6\uparrow}a^{\dagger}_{6\downarrow})(0.88a^{\dagger}_{2\uparrow}a^{\dagger}_{2\downarrow} - 0.48a^{\dagger}_{5\uparrow}a^{\dagger}_{5\downarrow}) \times\frac{1}{\sqrt{2}}(a^{\dagger}_{3\uparrow}a^{\dagger}_{4\downarrow} - a^{\dagger}_{3\downarrow}a^{\dagger}_{4\uparrow})|0>, \quad (3.7)$$



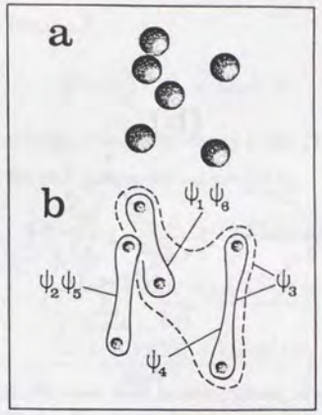


Figure 3.2: An example of the spin-triplet clusters. (a) The geometrical arrangement of six donor atoms. (b) MCSCF one-electron orbitals, shown only for $N_D = 1.7 \times 10^{18} cm^{-3}$.

while that of the first excited state is written as,

$$\Phi^{(ex)}_{Triplet} = (0.95a^{\dagger}_{1\uparrow}a^{\dagger}_{1\downarrow} - 0.31a^{\dagger}_{6\uparrow}a^{\dagger}_{6\downarrow})(0.88a^{\dagger}_{2\uparrow}a^{\dagger}_{2\downarrow} - 0.48a^{\dagger}_{5\uparrow}a^{\dagger}_{5\downarrow}) \times(0.76a^{\dagger}_{3\uparrow}a^{\dagger}_{3\downarrow} - 0.65a^{\dagger}_{4\uparrow}a^{\dagger}_{4\downarrow})|0> . \quad (3.8)$$

From these we can see that the spin pair model also holds in the present case. The ground state (3.7) consists of three spin pairs, two of which are spin-singlet states and one is a spin-triplet state. The triplet pair is formed by two electrons in $\psi_3$ and $\psi_4$. These same electrons form a spin-singlet pair in the first excited state (3.8). Since $\psi_3$ and $\psi_4$ have a symmetry property close to the E irreducible representation of the $C_{3v}$ point group, which is orbitally doubly degenerate, these one-electron orbitals are expected to be almost degenerate. In this context the appearance of spin-triplet ground states may be attributed to Hund's rule coupling of two electrons in two nearly degenerate orbitals, that is, spin-triplet ground states may simply be due to the symmetric arrangements of donors which happen to appear in a random distribution.

There seem to be two typical geometrical arrangements which produce a spin-triplet ground state in a random system. Fig.3.3 shows examples of the two typical geometries which give rise to Hund's rule coupling. At low donor concentration geometry (a) appears

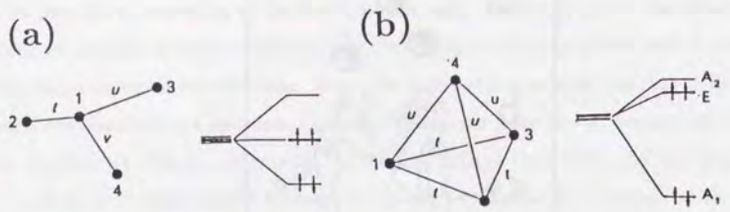


Figure 3.3: Two types of atomic configurations that have the spin-triplet ground states are shown together with their electronic energy levels and the electron occupancy for the half-filled case. (a) A cluster with appreciate transfer energies (t,u,v) only between the central atom and the surrounding atoms, (b) a cluster with the accidental symmetry of $C_{3v}$.

often, while at high concentration geometry (b) is more common. The cluster shown in Fig.3.2 corresponds to geometry (b).

For spin-triplet clusters the CI wavefunctions of the ground states are expressed by a small number of configurations, when the donor concentration is high. In the present case they approach the form of two Slater determinants;

$$\frac{1}{\sqrt{2}}\{|\psi_1\alpha\psi_1\beta\psi_2\alpha\psi_2\beta\psi_3\alpha\psi_4\beta| + |\psi_1\alpha\psi_1\beta\psi_2\alpha\psi_2\beta\psi_3\beta\psi_4\alpha|\},$$

near the MI transition.

## 3.4 Specific Heat and Spin-Susceptibility

Using the calculated results of the MCSCF-CI method the specific heat in magnetic fields and the spin-susceptibility are calculated as functions of temperature. First, we calculate these quantities for each cluster, assuming a canonical distribution. Then we take an ensemble average of these quantities over fifty clusters for each concentration.

The formulae which we have used are the following. In the presence of a magnetic field, $H$, the energy of the $n$-th many-body eigenstate has the Zeeman term shown below, if we



neglect the higher-order effects in $H$.

$$E(n, S_z) = E_n + 2\mu_B S_z H, \tag{3.9}$$

where $E_n$ is the n-th eigenenergy. Using the energy levels (3.8), the specific heat, $C$, and the spin-susceptibility, $\chi$, for each cluster are calculated by,

$$\begin{aligned} C/k_B &= \sum_n \sum_{S_z=-S_n}^{S_n} \{\frac{E(n,S_z)}{k_BT}\}^2 \frac{\exp(-E(n,S_z)/k_BT)}{Z} \\ &\quad -\{\sum_n \sum_{S_z=-S_n}^{S_n} \frac{E(n,S_z)}{k_BT} \frac{\exp(-E(n,S_z)/k_BT)}{Z}\}^2, \end{aligned} \tag{3.10}$$

$$\chi/4\mu_B^2 = \sum_n \frac{S_n(S_n+1)(2S_n+1)}{3k_BT} \frac{\exp(-E_n/k_BT)}{Z}, \tag{3.11}$$

where Z is the partition function for a canonical ensemble,

$$Z = \sum_n \sum_{S_z=-S_n}^{S_n} \exp(-E(n,S_z)/k_BT). \tag{3.12}$$

$\mu_B$ is the Bohr magneton, $k_B$ is the Boltzmann constant and $S_n$ is the total spin of the $n$-th level.

Figure 3.4 shows the temperature dependence of the specific heat for several values of magnetic field for four donor concentrations. The specific heat of a single cluster seems to be the superposition of several Schottky-type specific heats. However, when the specific heat is averaged over fifty samples, it becomes linear in T in the high temperature region for $N_D$ larger than $1.7 \times 10^{18} cm^{-3}$. This T-linear behavior is due to the randomness of the energy spectrum in each cluster. At low temperatures, about 1 K, a hump over the T-linear part is seen in the specific heat, whose position corresponds to the average value of the first excitation energy for each concentration. This reflects the effect of the spin-dependent intersite interactions which form the spin pairs. This coincides with Takemori and Kamimura's argument that the hump is ascribed to the Schottky-type peak and corresponds to the thermal excitation between spin-singlet and spin-triplet states in a spin pair [26]. The features of the specific heat mentioned above are in good agreement with experimental results [33,34,35]. However, the size of the hump increases with increasing a donor concentration. This disagrees with experimental results, and it may be due to a finite size effect of the clusters.

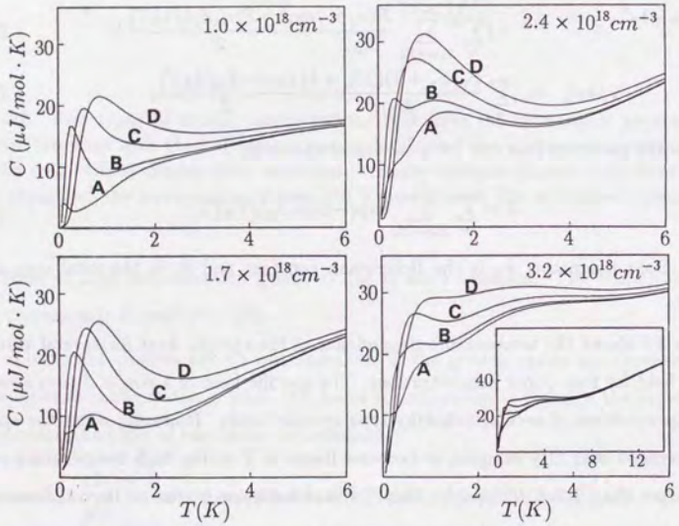


Figure 3.4: Temperature dependence of the specific heat averaged over fifty clusters for each donor concentration. The magnetic fields correspond to 0 kOe (curve A), 5 kOe (curve B), 10 kOe (curve C) and 15 kOe (curve D), respectively.



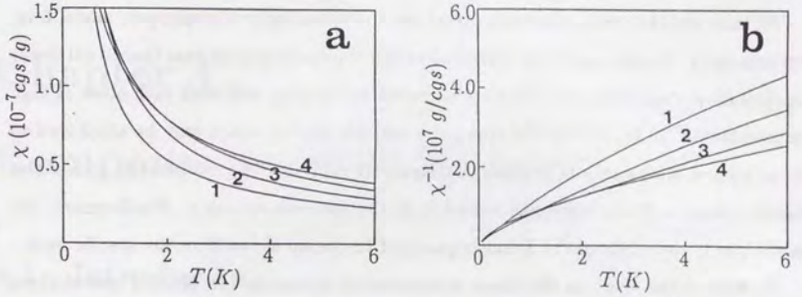


Figure 3.5: (a) Temperature dependence of the spin-susceptibility averaged over fifty clusters. The donor concentrations are 1.0 $\times 10^{18} cm^{-3}$ (curve 1), 1.7 $\times 10^{18} cm^{-3}$ (curve 2), $2.4 \times 10^{18} cm^{-3}$ (curve 3), and $3.2 \times 10^{18} cm^{-3}$ (curve 4), respectively. (b) The Curie-Weiss plots of the spin-susceptibility for four concentrations.

When the donor concentration is low, the specific heat, in particular its hump, changes drastically with magnetic fields at low temperatures. The hump over the T-linear part coincides with the shape of a Schottky-type peak. Its position is shifted to higher temperatures with increasing magnetic field. This peak corresponds to the Zeeman splitting of a ground state in spin-triplet clusters. With increasing concentration, the change in the specific heat between the presence and absence of magnetic fields decreases. This behavior is also in good accordance with experimental results [35].

The spin-susceptibility and its Curie-Weiss plot are shown in Fig.3.5. The susceptibility diverges to infinite with decreasing T as in a paramagnet because of the existence of spin-triplet clusters. The Curie-Weiss plots are almost T-linear (Curie type) with a downward bending at low temperatures, again consistent with experimental results [28,36,37,38,39,40].

## 3.5 Conclusion and Remarks

We have calculated the electronic states in the uncompensated system of Si:P by the MCSCF-CI method, using a cluster model. We have shown that the representation based

on the MCSCF one-electron orbitals is very useful for investigating the features of the electronic states in the Anderson-localized region of Si:P.

We have elucidated the electronic structure corresponding to the spin pair model from first principles. Namely, pair-type correlation effect is important even near the critical donor concentration, even if the spin pairs are extended and overlap well with each other at high concentrations. 10 to 20 % of the spin pairs are spin-triplet, which may be attributed to the accidental appearance of two nearly degenerate orbitals. The existence of spin-triplet clusters causes a Curie-Weiss-like behavior in the spin-susceptibility. Furthermore, the results clarify the origin of the T-linear part and the hump at low T in the specific heat.

We have noted that, as the donor concentration increases, the MCSCF one-electron orbitals near the Fermi level become more extended, while the CI wave functions approach the form of a single Slater determinant for spin-singlet clusters, and that of two Slater determinants for spin-triplet clusters. This means that, with increasing donor concentration, the electron correlation decreases because the electron-electron interactions are screened more effectively by the more extended MCSCF one-electron orbitals. This suggests that the metal-insulator transition in doped semiconductors has the nature of a Mott-type transition. On the other hand, some MCSCF one-electron orbitals at lower energy remain localized in a real space even at the critical donor concentration. This implies the importance of the random effect. In this context we conclude that the mechanisms of both Anderson- and Mott-type MI transitions cooperate in the metal-insulator transition in doped semiconductors.

In spite of the finite system size of N=6, the experimental results of the specific heat and the spin-susceptibility can be explained well by the present simulation. This suggests that the local properties of the electronic states can be described well in this cluster simulation, although it is not directly applicable to transport properties or other quantities which are sensitive to boundary conditions.



# Chapter 4

# Compensated Si:P Systems

## 4.1 Introduction

It is well known that various properties of doped semiconductors are influenced by compensation. For example, in the low doping concentration region the features of the hopping conduction have been investigated theoretically [41,42]. Its behavior changes by the compensation ratio, which is defined as the ratio of the number of the minority carriers to that of the majority carriers doped in the semiconductor. Some of the theories on hopping conduction have taken into account the effect of electron-electron interactions, and suggested the appearance of a gap in the density of states at the Fermi level in the presence of compensation. This is called the Coulomb gap. It has been predicted that the existence of the Coulomb gap induces the change in the exponent of the variable range hopping, which should be observed at low temperatures. This prediction has stimulated many experimentalists to investigate the hopping behavior.

The metal-insulator transition occurs at almost the same electron concentration in the compensated system as in the uncompensated system. However, its critical behavior may be changed by the compensation. The critical exponent $\nu$ of the conductivity, $\sigma(T=0) = \sigma_0(n/n_c - 1)^{\nu}$, is 0.5 in the uncompensated Si:P while it seems to be 1.0 in all the other doped semiconductors, including the compensated Si:P, according to experimental reports [43,44]. This feature has not been explained yet.

In the intermediate concentration region some other properties of the compensated semiconductors have been reported to be different from those of the uncompensated samples. For example, the specific heat of electrons behaves as T-linear at low temperatures, even in

the low concentration regions in the compensated Si:P, while this T-linear behavior disappears in the low concentration region in the uncompensated Si:P [45]. As for the magnetic properties, the line width of ESR measurements becomes wider with the compensation.

In spite of several experimental works on compensated doped semiconductors in the intermediate to the critical concentration region, there have been few theoretical works on the Anderson-localized states in the compensated systems. It is necessary to study the electronic structures from the microscopic point of view to clarify the different features between the uncompensated and the compensated doped semiconductors. In this chapter we calculate the electronic structure in the compensated Si:P system for the purposes listed below.

(1) We clarify the electronic states from the low to the intermediate concentration region. Then we elucidate the characteristic features of the electronic structure in compensated Si:P, and compare with the electronic structure in the uncompensated system discussed in the previous chapter.

(2) We calculate the T-dependence of the specific heat in magnetic fields, and the spin-susceptibility and explain the differences from those of the uncompensated Si:P.

In the calculation we take, as a model, a cluster consisting of donors and acceptors, both of which are distributed randomly in a sphere. We approximate the acceptors as point charges for the low temperature region. The Hamiltonian of this system can be written in the effective mass approximation as,

$$H = \sum_k (\frac{1}{2}\mathbf{p}_k^2 - \sum_\nu \frac{1}{|\mathbf{r}_k - \mathbf{R}_\nu|} + \sum_\mu \frac{1}{|\mathbf{r}_k - \mathbf{R}_\mu|}) + \sum_{k>l} \frac{1}{|\mathbf{r}_k - \mathbf{r}_l|}, \qquad (4.1)$$

where $\nu$ and $\mu$ represent the donor and acceptor sites, respectively. We evaluate the electronic states by the MCSCF and the CI method to take account of the correlation effect. Further, we calculate the specific heat and the spin-susceptibility in the same way as described in chapter 3.

In section 4.2 we explain the cluster model and the calculation method. We present the simulated results in section 4.3 and the calculations of the specific heat and the spin-susceptibility in 4.4. A summary and discussions are given in section 4.5.



| Case | Cluster | | | Concentration ( $\times 10^{18} cm^{-3}$ ) | | |
|---|---|---|---|---|---|---|
| | electron | donor | acceptor | electron | donor | acceptor |
| a | 4 | 8 | 4 | 1.5 | 3.0 | 1.5 |
| b | 4 | 12 | 8 | 1.0 | 3.0 | 2.0 |
| c | 4 | 8 | 4 | 1.0 | 2.0 | 1.0 |
| d | 4 | 8 | 4 | 0.25 | 0.5 | 0.25 |

Table 4.1: The number of electrons, donors and acceptors in the clusters we have selected for the calculation. The concentrations corresponding to the clusters are also listed.

## 4.2 Cluster Calculation Method

We choose clusters with four electrons, consisting of 8 (or 12) donors and 4 (or 8) acceptors distributed randomly in a sphere. The concentrations we consider are listed in Table 4.1. Cases a, b and c are in the intermediate doping region, while case d corresponds to the low concentration region. The ratio of acceptors to donors, the concentration ratio, is 1/2 in cases a, c and d, and is 2/3 in case b. A Gaussian-type hydrogen 1s orbital is attached to each donor site. The exponent is chosen to $8/9\pi$ as in chapter 3. Acceptors are represented by point charges of charge $-e$.

In the MCSCF method we consider all the configurations of the pair-type excitations. For example, in case a in Table 4.1, the MCSCF trial function is given as,

$$\begin{aligned} \Phi_{MCSCF} &= \tilde{C}_0 \Psi_0 + \sum_{i=1}^{2} \sum_{a=3}^{8} \tilde{C}_{ii}^{aa} \Psi_{ii}^{aa} \\ &= (\tilde{C}_0 + \sum_{i=1}^{2} \sum_{a=3}^{8} \tilde{C}_{ii}^{aa} a_{a\uparrow}^\dagger a_{a\downarrow}^\dagger a_{i\downarrow} a_{i\uparrow}) \Psi_0, \end{aligned} \qquad (4.2)$$

where $\Psi_0 = |\psi_1 \alpha \psi_1 \beta \psi_2 \alpha \psi_2 \beta|$. The one-electron orbitals $\{ \psi_k, k = 1, \cdots, 8 \}$ are determined in the variational procedure. Next we carry out the CI calculation based on the MCSCF one-electron orbitals, to include all the electron-electron interactions.

The calculations are done for thirty clusters for each case.

For comparison in the low concentration region, we perform the cluster calculations for the uncompensated system at the concentration of $N_D = (0.5, 0.25) \times 10^{18} cm^{-3}$. We take the cluster model consisting of 6 randomly distributed donors in the same way as in the previous chapter.

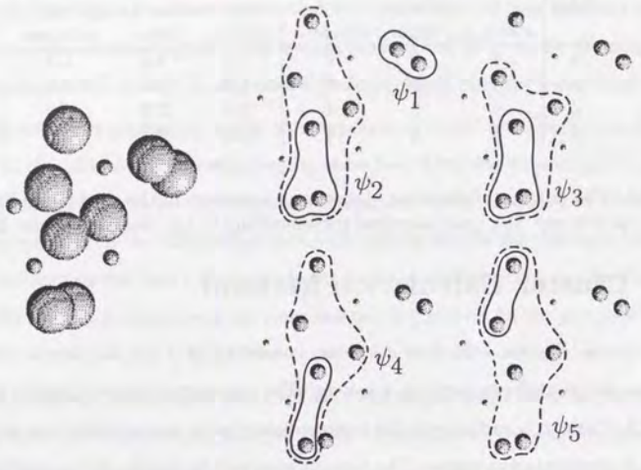


Figure 4.1: An example of the spin-singlet clusters. The concentration corresponds to case a in Table.4.1. The large and the small spheres represent the donors and the acceptors, respectively. The solid and broken lines indicate the highest and the lowest amplitudes of the MCSCF orbitals, respectively.

## 4.3 Calculated Results

We present in the following the calculated results in our cluster simulations.

Most of the clusters have the spin-singlet ground states. The proportion of the spin-triplet clusters is 10 to 20 % in the intermediate concentration region, which is almost the same as that of the uncompensated system. At low concentration the ground state becomes spin-degenerate in many clusters.

One example of the spin-singlet clusters is shown in Fig.4.1 for the concentration of case a in Table 4.1, which belongs to the intermediate doping concentration region. The MCSCF one-electron orbitals are more extended than those in the uncompensated system at the same electron concentration. The extension of the one-electron orbitals does not change very much when the concentration decreases, which is also in contrast to the uncompensated system.

The CI wavefunctions of the ground and the first excited states are given, respectively,



as,

$$\Phi_g = 0.93|\psi_1\alpha\psi_1\beta\psi_2\alpha\psi_2\beta| - 0.29|\psi_1\alpha\psi_1\beta\psi_3\alpha\psi_3\beta| \\ -0.19|\psi_1\alpha\psi_1\beta\psi_4\alpha\psi_4\beta|, \tag{4.3}$$

and

$$\Phi_{ex} = 0.65\{|\psi_1\alpha\psi_1\beta\psi_2\alpha\psi_3\beta| + |\psi_1\alpha\psi_1\beta\psi_2\beta\psi_3\alpha|\} \\ -0.14\{|\psi_1\alpha\psi_1\beta\psi_2\alpha\psi_4\beta| + |\psi_1\alpha\psi_1\beta\psi_2\beta\psi_4\alpha|\} \\ -0.16\{|\psi_1\alpha\psi_1\beta\psi_2\alpha\psi_5\beta| + |\psi_1\alpha\psi_1\beta\psi_2\beta\psi_5\alpha|\}. \tag{4.4}$$

The ground state wavefunction, (4.3), is much closer to a single Slater determinant, compared with the CI wavefunction (3.3) of the uncompensated system. It indicates that the one-electron picture is almost valid in this system and that the correlation effect is much weaker than that in the uncompensated system. This is because the more extended MCSCF one-electron orbitals screen the Coulomb interactions more strongly.

The first excited state is a spin-triplet which consists of six electron configurations, as seen in (4.4). The first two configurations in (4.4), which have the largest coefficients, come from the spin-dependent interaction between the orbital $\psi_2$ and $\psi_3$, just as in the spin pair model. The other four configurations in (4.4) correspond to hopping type excitations; an electron is excited from $\psi_2$ to the orbitals, $\psi_4$ or $\psi_5$, which are localized around the other donors. This has the effect that an electron moves to some other place from the localized region in the ground state. In this view spin coupling effect is not as strong in the compensated system as in the uncompensated system, where the spin coupling is very important.

The cases b and c correspond to the same electron concentration but with a different compensation ratio. Although the MCSCF orbitals in case b are a little more extended than in case c, the features discussed above are almost the same in both cases.

Now we discuss the low concentration region in the uncompensated and the compensated systems. As the concentration decreases, electrons become localized and the spin coupling effect diminishes in both systems. In the uncompensated system the excitation energy from the almost spin-degenerate ground state increases drastically. This is due to

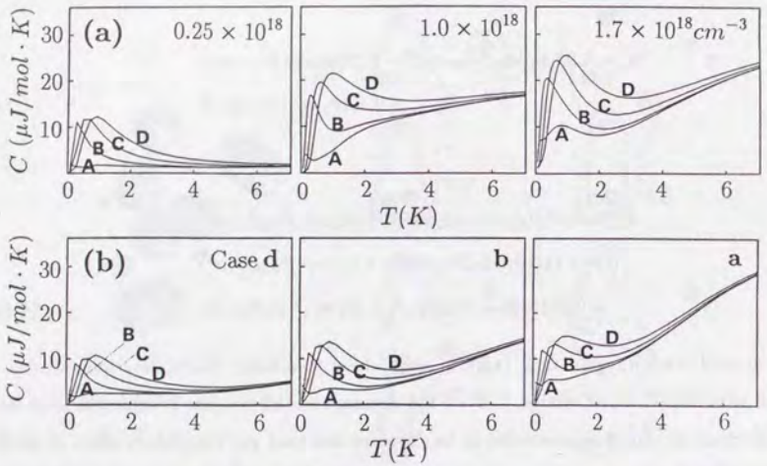


Figure 4.2: The temperature dependence of the specific heat averaged over thirty clusters. The upper row, (a), corresponds to the uncompensated case while the lower row, (b), to the compensated case. The values of the magnetic field are 0 (curve A), 5 KOe (curve B), 10 KOe (curve C) and 15 KOe (curve D), respectively.

the intra-state interaction, that is, Hubbard U repulsion, which becomes larger in the more localized states. In the compensated system, on the other hand, hopping-type excitations exist above the nearly spin-degenerate ground state. This delocalizes the electrons and hence the excitation energy is much smaller.

## 4.4 Specific Heat and Spin-Susceptibility

We calculate the temperature dependence of the specific heat in magnetic fields and the spin-susceptibility in the same way as in the previous chapter. First, we calculate the quantities for each cluster and then take an ensemble average over 30 clusters for each case in Table 4.1.

Fig.4.2 shows the T-dependence of the specific heat under several values of the magnetic field. The lower figures show the results of the compensated system while the upper figures show the results of the uncompensated system corresponding to the same electron concen-



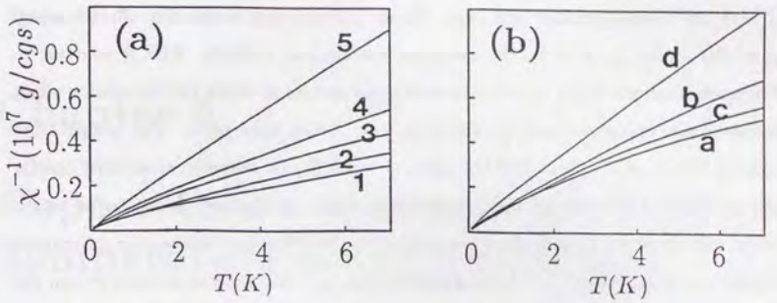


Figure 4.3: Curie-Weiss plots of the spin-susceptibility averaged over thirty clusters; (a) the uncompensated systems and (b) the compensated systems. In (a) the donor concentrations correspond to $N_D = 2.4$ (curve **1**), 1.7 (curve **2**), 1.0 (curve **3**), 0.5 (curve **4**), $0.25 \times 10^{18} cm^{-3}$ (curve **5**). In (b) the concentrations correspond to case a, b, c and d in Table.4.1.

trations. In the intermediate concentration region the specific heat behaves in the similar way in both systems: T-linear in the higher temperature region and a hump over the T-linear part is seen at low temperatures. However, the hump is smaller in the compensated system, which reflects the weaker spin-dependent interaction.

In the low concentration region the specific heat shows a T-linear behavior only in the compensated system. This is attributed to the hopping-type excitations. The gradient is an increasing function of dopant concentration while the hump becomes smaller as the concentration decreases. These results are in accordance with experiments [45].

In Fig.4.3 the Curie-Weiss plots of the spin-susceptibility are shown for the uncompensated and the compensated systems. The T-dependence of the susceptibility is qualitatively the same between both systems. It tends to diverge with decreasing T even in the intermediate concentration. This is due to the existence of spin-triplet clusters.

## 4.5 Conclusion and Remarks

We have calculated the electronic structure in the compensated Si:P system by the MCSCF-CI method. In the intermediate concentration region the MCSCF one-electron orbitals are

more extended and the CI wavefunction is much closer to a single Slater determinant, compared with the uncompensated Si:P case. These indicate that correlation effect is small owing to the screening effect by the extended one-electron orbitals. This is contrast to the Anderson-localized states in the uncompensated system in which the correlation effect is fundamentally important and the electrons form strong spin pairs. The temperature dependence of the specific heat and the spin-susceptibility is, however, essentially similar in both systems in the intermediate concentration region. In the low concentration region where the spin-dependent interactions become small, the difference between the uncompensated and the compensated Si:P becomes more obvious. The excitation energy from the almost spin-degenerate ground state increases drastically in the former, while hopping-type excitations with small excitation energies exist in the latter. As a consequence, the specific heat behaves as T-linear only in the compensated system.

We cannot predict the transport properties, like the hopping conduction, directly by this finite cluster calculations. For that we must develop a simpler and much larger model. As for the Coulomb gap, we also need to treat a larger system because the gap is caused by the long range nature of the Coulomb interactions.



# Chapter 5

# Copper Oxide Materials of High Temperature Superconductors

## 5.1 Introduction

Since high-temperature copper-oxide superconductors were discovered, intensive studies have been done on the mechanism of the superconductivity. The materials may be classified as strongly correlated systems and thus the band picture is not suitable. In fact, most of the band structure calculations for these materials have not been able to explain the observed anti-ferromagnetic insulating property in the undoped compounds [8,9,10,11]. Here, the problem is how to treat the strong correlation in order to elucidate the electronic states in the normal phase as well as the mechanism of the superconductivity.

To study strong correlation effect in these systems, a number of simulation studies have been done based on the Hubbard model, the t-J model, *etc.* [5,6]. In these simulation studies, however, important physical quantities such as transfer integrals, energy differences between orbitals, have been taken as parameters. In order to elucidate the electronic structures of the copper oxide superconductors, it is necessary to calculate all physical quantities from first principles.

The copper oxide compounds of high-temperature superconductors have a couple of common features. They all have $CuO_2$ planes which are thought to be important for the superconductivity. There are some additional Cu-O structures, octahedron, pyramid *etc.*, according to the number of apical oxygens above and below a copper atom in the $CuO_2$ plane. The undoped compounds are anti-ferromagnetic insulators. However, they show

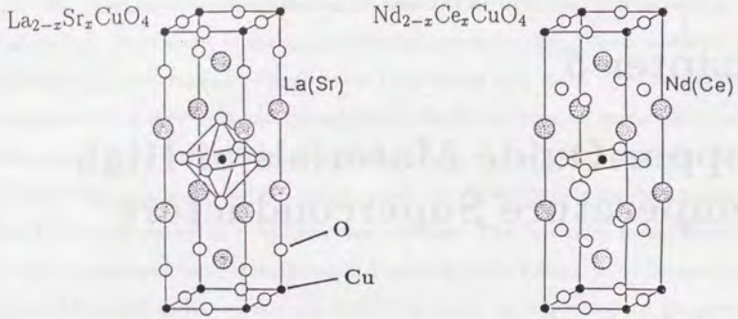


Figure 5.1: The crystal structures of the La-Cu-O and the Nd-Cu-O systems. The former has the octahedron structure while the latter has no apical oxygens.

superconductivity when carriers are doped by the substitution of divalent or tetravalent ions in place of the trivalent ions, or by oxygen vacancies. In this chapter we study two compounds among them, $La_{2-x}Sr_xCuO_4$ and $Nd_{2-x}Ce_xCuO_4$. The La-Cu-O system has an elongated octahedron structure while Nd-Cu-O has no apical oxygens above or below the $CuO_2$ plane, as seen in Fig.5.1. The former becomes superconducting when holes are doped while the latter becomes superconducting when electrons are doped.

In order to calculate the electronic structures of these materials from first principles, we adopt the MCSCF-CI method from the standpoint that the correlation effect plays a major role in these materials. To elucidate the electronic structure in the $CuO_2$ plane, we take as a model clusters consisting of one or two copper atoms with the surrounding oxygen atoms. Although some other groups have already performed *ab initio* calculations in similar cluster models [46,47,48], we place special emphasis on the following points in our calculations, which have not received sufficient attention previously.

(1) In order to clarify the correlation effect characteristic of these materials, we represent the electronic states in a number of Slater determinants by the MCSCF-CI method. The small number of configurations by this method allows us to investigate the origin of the



anti-ferromagnetic coupling in the undoped compounds and the properties of the electronic states in the carrier-doped compounds.

(2) We calculate the electronic states in both the La-Cu-O and the Nd-Cu-O systems with the same formalism and elucidate the essential differences between the hole-doped and electron-doped superconductors.

(3) We investigate the role of the apical oxygens in the La-Cu-O system. Recently, there have appeared experimental results suggesting that the distance between the apical O atom and the Cu atom is reduced when carriers are doped in the high temperature superconducting copper-oxide materials [49,50]. As for the $La_{2-x}Sr_xCuO_4$ compounds, Boyce *et al.* have found, by X-ray absorption studies, that the distance becomes shorter as the doping concentration of Sr increases [50]. Theoretically, Shima *et al.* have shown, by total energy-force calculations, that the optimized Cu–apical O distance becomes shorter with increasing doping concentration [51]. In addition, there are experimental reports that the onset temperature of the superconductivity ($T_c$) rises under high pressure in high temperature superconductors, except in the Nd-Cu-O system which has no apical oxygens [52,53]. This fact also implies the importance of the apical oxygens for the superconductivity. To investigate the effect of the apical oxygens, therefore, we vary the Cu–apical O distance in the cluster model.

(4) We will study the influence on the electronic structure of the doped divalent or tetravalent ions.

The organization of this chapter is as follows. In the next section we present the cluster model and the calculation method. We give the calculated results in the $CuO_6$ and the $CuO_4$ clusters in section 5.3 and 5.4, respectively. In section 5.3 we elucidate the effect of the apical oxygens in the La-Cu-O system. Section 5.5 is devoted to the calculated results in the $Cu_2O_{11}$ and the $Cu_2O_7$ clusters. We investigate the anti-ferromagnetic coupling by the superexchange mechanism there. We give a summary and some discussions in section 5.6.

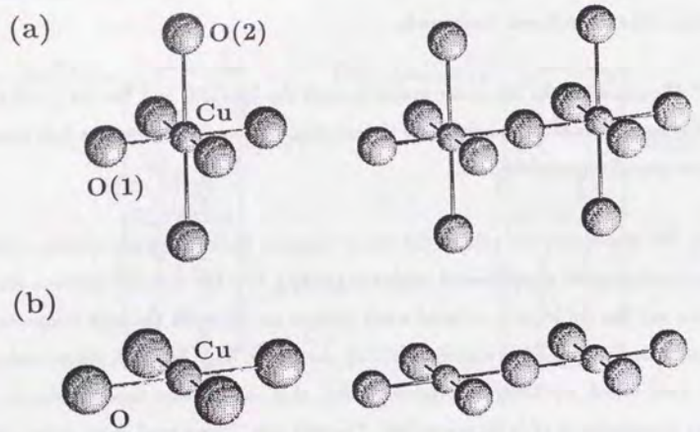


Figure 5.2: The clusters we take as a model in the calculations; (a) $CuO_6$ and $Cu_2O_{11}$ for La-Cu-O, (b) $CuO_4$ and $Cu_2O_7$ for Nd-Cu-O.

## 5.2 Cluster Calculation Method

### 5.2.1 Cluster Model

As a model we adopt clusters of $CuO_6$ and $Cu_2O_{11}$ for La-Cu-O, and $CuO_4$ and $Cu_2O_7$ clusters for Nd-Cu-O, as shown in Fig.5.2. $CuO_6$ and $Cu_2O_{11}$ clusters include two kinds of oxygens; oxygen in the $CuO_2$ plane, which we call O(1) hereafter, and apical oxygen above and below the Cu atoms in the direction of c-axis, which we label as O(2). The $CuO_4$ and $Cu_2O_7$ clusters include only one kind of oxygen atoms, O(1). The lattice constants we use are listed in Table 5.1. The number of electrons is determined so that the charge of copper is +2 and that of oxygen is −2 for the undoped case. We also consider the hole-doped system for La-Cu-O, and the electron-doped system for Nd-Cu-O by subtracting, and adding, one electron, respectively.

To include the effect of the Madelung potential from the exterior ions outside the cluster, point charges are placed at exterior ion sites (+2 for Cu, −2 for O and +3 for La (Nd)). Fractional charges are given to the most outer La (Nd) ion sites in such a way that the



| | Cu–O(1) | Cu–O(2) |
|---|---|---|
| $La_2CuO_4$ | 1.889 | 2.411 |
| $Nd_2CuO_4$ | 1.973 | |

| | Ni–O |
|---|---|
| NiO | 2.0973 |

Table 5.1: The lattice constants of $La_2CuO_4$, $Nd_2CuO_4$ and NiO. The length is indicated in angstroms. We use the values of the lattice constants in Ref.[54] for $La_2CuO_4$, Ref.[55] for $Nd_2CuO_4$ and Ref.[56] for NiO.

effect up to electronic octapoles disappears at the ions located far away from the cluster. The number of point charges are 168 for $CuO_6$, 224 for $Cu_2O_{11}$, 208 for $CuO_4$ and 276 for $Cu_2O_7$. These point charges define the Madelung potential at Cu, O(1) and O(2) sites of the clusters in such a way that the relative value of the Madelung potential at each site is reproduced to coincide with that in the purely ionic crystal, to within less than 0.8 %. The whole system is electrically neutral for the undoped case and we assume that the arrangement of point charges does not change when a hole or an electron is added, except in subsection 5.3.3 and 5.4.3, where we investigate the effect of doping with $Sr^{2+}$ or $Ce^{4+}$ ions.

In accordance to the suggestions from both the experimental result from the X-ray absorption study by Boyce *et al.*[50], and the theoretical study of the LDA total energy-force calculation by Shima *et al.* for $La_{2-x}Sr_xCuO_4$ [51], we vary the Cu–O(2) distance $c$ in $CuO_6$ cluster while the other lattice constants are kept fixed. The distance $c$ is taken as 2.41 Å, 2.35 Å, 2.30 Å and 2.24 Å, where 2.41 Å and 2.30 Å correspond to those of the undoped and 20% Sr doped systems, respectively [50]. The positions of the −2e point charges at O(2) sites outside the cluster are also changed by the same amount. The change in the lattice constant $c$ brings about the change in the electrostatic Madelung site potential in the purely ionic crystal. We calculate the Madelung potential as a function of $c$ by Ewald's method, and list the results in Table 5.2. As the O(2) is moved closer to the $CuO_2$ plane, the absolute values of the Madelung potential at the Cu and the O(2) sites become larger, while the potential at O(1) site becomes smaller. This means that an electron goes to an

| | Cu (or Ni) | O(1) | O(2) |
|---|---|---|---|
| $La_2CuO_4$ | | | |
| $c$=2.41Å | −28.44 | 21.26 (49.69) | 20.08 (48.52) |
| $c$=2.30Å | −29.53 | 20.49 (50.02) | 20.35 (49.89) |
| $Nd_2CuO_4$ | −24.30 | 22.14 (46.44) | |
| NiO | −24.40 | 24.40 (47.99) | |

Table 5.2: The electrostatic Madelung potential at the Cu (or Ni), O(1) and O(2) sites, in $La_2CuO_4$, $Nd_2CuO_4$ and NiO (in eV). The oxygen sites' potential, measured from that at the Cu (or Ni) site, is also indicated in the parentheses.

O(2) site more easily, and to an O(1) site more difficultly and that a hole goes to a Cu site more easily, as $c$ decreases.

For comparison we perform similar cluster calculations for NiO, which is an antiferromagnetic insulator of the sodium chloride structure. The lattice constant is shown in Table.5.1. We take a $NiO_6$ regular octahedron cluster and a $Ni_2O_{11}$ cluster with 336 and 428 point charges outside of the clusters, respectively.

### 5.2.2 Basis set

We express the one-electron orbitals by linear combinations of atomic orbitals (LCAO). The functional forms of the atomic orbitals are taken as linear combinations of Gaussian functions. For Cu 1s, 2s, 3s, 2p, 3p and O 1s we prepare one basis function for each orbital (single zeta), and for Cu 3d, 4s and O 2s, 2p we prepare two basis functions for each orbital (double zeta). ( (12s6p4d)/[5s2p2d] for Cu [57] and (10s5p)/[3s2p] for O [58])

With the oxygen ions, diffuse components are usually used in addition to the double or triple zeta functions in the field of quantum chemistry. This is because $O^{2-}$ is not stable by itself and is very much extended in space. Although other people use the diffuse components in their cluster calculations of the copper-oxide superconductors [46,47,48], we don't adopt them for the following reasons.

(i) In a molecule, electronic orbitals may be hybridized all over the molecule. Thus diffuse components become necessary to represent the electronic states in a molecule. We



would, however, like to simulate the electronic structure in a crystal where the electronic state in some neighborhood of an atom is expected to be closely represented by its atomic orbitals. Consequently, on physical grounds, we would not expect the diffuse components to be significant.

(ii) In addition, without the unphysical diffuse components, we may represent the Madelung potential simply with the point charge approximation in the outside region of the cluster.

Instead of using the diffuse components for $O^{2-}$, we make extended O 2p basis functions which were originally prepared for a neutral atom. For this purpose we introduce a scaling factor of 0.93 so that the orbitals scale up 1/0.93 times as extended in space as the original base. We multiply all the Gaussian exponents in the double zeta base for the oxygen 2p orbitals, by the same scaling factor, on the assumption that the shape of the orbitals is not changed from that in a neutral oxygen atom. Then the value of the scaling factor is determined so that the energy of an isolated $O^{2-}$ ion should be minimized in the Hartree-Fock approximation.

For the same reason the 3d orbitals are shrunk in a $Cu^{2+}$ ion, compared to those in a neutral Cu atom. For this we introduce a scaling factor of 1.09 so that the Cu 3d orbitals scales down 1/1.09 times. Again, the scaling factor is determined so that the HF energy of isolated $Cu^{2+}$ ion should be minimized.

For Ni atom, we take the basis set similar to that for Cu atom; single zeta for 1s, 2s, 3s, 2p, 3p and double zeta for 3d, 4s ((12s6p5d)/[5s2p2d] in Ref.[59]).

### 5.2.3 Calculation of MCSCF-CI Method

In the calculations of hole-doped $CuO_6$ and electron-doped $CuO_4$ systems we perform the MCSCF-CI variational calculations for both the $^1A_{1g}$ and the $^3B_{1g}$ states independently. In the MCSCF method we take the trial function for the $^1A_{1g}$ state as

$$\begin{aligned}\Phi_S &= \tilde{C}_0|\psi_1\alpha\psi_1\beta\psi_2\alpha\psi_2\beta\cdots\psi_n\alpha\psi_n\beta| \\ &+ \sum_i\sum_a \tilde{C}_i^{aa}|\cdots\psi_{i-1}\alpha\psi_{i-1}\beta\psi_{i+1}\alpha\psi_{i+1}\beta\cdots\psi_a\alpha\psi_a\beta|, \qquad (5.1)\end{aligned}$$

and that for the $^3B_{1g}$ state as

$$\Phi_T = \tilde{C}_0|\psi_1\alpha\psi_1\beta\cdots\psi_{n-1}\alpha\psi_{n-1}\beta\psi_p\alpha\psi_q\alpha| + \sum_i\sum_a \tilde{C}_{ii}^{aa}|\cdots\psi_{i-1}\alpha\psi_{i-1}\beta\psi_{i+1}\alpha\psi_{i+1}\beta\cdots\psi_a\alpha\psi_a\beta\psi_p\alpha\psi_q\alpha|, \quad (5.2)$$

where $2n$ is the number of the electrons in the cluster. $\psi_p$ and $\psi_q$ in (5.2) correspond to the singly-occupied orbitals of Cu $d_{3z^2-r^2}$ and $d_{x^2-y^2}$ character, respectively. The summations over $i$ and $a$ are taken over all the $a_{1g}$ and $b_{1g}$ symmetry orbitals of the $D_{4h}$ point group, which consist of Cu 3d, 4s and O 2p orbitals. We also perform the CI calculations for the $^1A_{1g}$ and the $^3B_{1g}$ states using the $^1A_{1g}$ and the $^3B_{1g}$ MCSCF one-electron orbitals, respectively. In the CI calculation we include all the excitations among these orbitals. (There are too many molecular orbitals to consider the full configuration space in the capacity of the present computer.)

We perform the calculations in the undoped $Cu_2O_{11}$ and $Cu_2O_7$ clusters in a similar way. We explain the calculation method in detail in section 5.5.

## 5.3 $CuO_6$ Cluster

### 5.3.1 Undoped system

First we present the electronic state in undoped $CuO_6$ cluster which includes 87 electrons. We carry out the unrestricted Hartree-Fock (UHF) calculation for the spin-doublet state. In the UHF calculation the orbitals of up-spin can be changed from those of down-spin, and thus a part of the correlation effect is effectively taken into account.

In the calculated result, the $b_{1g}$-type orbital in which Cu $d_{x^2-y^2}$ and O(1) $p_\sigma$ are coupled in an anti-bonding way is singly-occupied. That is, the hole is extended over the Cu and the O sites. As a result, the formal charge of the Cu site, which is estimated by the Mulliken analysis, is much reduced from +2, as seen in Table 5.3. The electronic state in the undoped cluster changes little when the Cu–O(2) distance is reduced.

For comparison, we perform the $NiO_6$ cluster calculation for NiO. NiO has regular octahedral symmetry so that the ground state is a spin-triplet owing to Hund's coupling. Thus we perform the UHF for the spin-triplet state. The $a_{1g}$ and the $b_{1g}$ orbitals are singly-occupied, in which the amplitudes of the Ni d orbitals are large and the hybridization with



| Cluster | Cu (or Ni) | O(1) | O(2) |
|---|---|---|---|
| undoped $CuO_6$ ($La_2CuO_4$) | 1.27 | −1.87 | −1.90 |
| undoped $CuO_4$ ($Nd_2CuO_4$) | 1.84 | −1.96 | |
| $NiO_6$ (NiO) | 1.74 | −1.96 | |

Table 5.3: The Mulliken charges in the undoped $CuO_6$ ($La_2CuO_4$), the undoped $CuO_4$ ($Nd_2CuO_4$) and the $NiO_6$ cluster (NiO). The calculations are done by the unrestricted HF method for the spin-doublet state (in $La_2CuO_4$ and $Nd_2CuO_4$) and for the spin-triplet state (in NiO).

the O $p_\sigma$ is small. It indicates that the two holes are localized at the Ni site in $NiO_6$ cluster in contrast to that in the undoped $CuO_6$ system. This is reflected in the Mulliken charges listed in Table 5.3. The formal charge of the Ni site is close to +2.

This indicates that covalency is important in $La_2CuO_4$ while the ionicity is strong in NiO.

### 5.3.2 Hole-doped System

When one electron is subtracted from the undoped $CuO_6$ cluster, the states of the $^1A_{1g}$ and the $^3B_{1g}$ symmetry of the $D_{4h}$ group are almost degenerate, as seen below. We perform the MCSCF-CI calculations for those states independently to determine which state is the ground state as a function of the Cu–O(2) distance. First, we present the electronic structures of the $^1A_{1g}$ and the $^3B_{1g}$ states. Then we compare the energies of these states. After that, we investigate the states of other symmetries.

(1) $^1A_{1g}$ State

The wavefunctions and one-electron orbitals in the MCSCF-CI results are shown in Fig.5.3 and 5.4, respectively. The CI wavefunction mainly consists of three configurations. It is close to a single Slater determinant and it indicates that the correlation effect is small. In the first configuration, which has the largest coefficient, the Cu $d_{x^2-y^2}$–O(1) $p_\sigma$ anti-bonding $b_{1g}$ orbital, $\psi_5$, is unoccupied. In the second configuration, the bonding orbital, $\psi_4$, is unoccupied while the anti-bonding orbital, $\psi_5$, is doubly occupied. Thus the mixing between the first and the second configurations indicates that the added hole enters both of the Cu $d_{x^2-y^2}$ and the O(1) $p_\sigma$ orbitals and that the added hole makes a spin-singlet pair

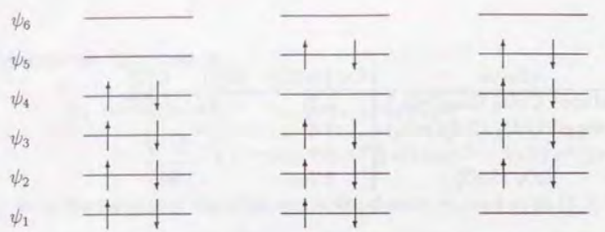


| | | | | |
|---|---|---|---|---|
| | | | | Cu 4s |
| | | | | Cu $d_{x^2-y^2}$ |
| | | | | O(1) $p_\sigma$ ($b_{1g}$) |
| | | | | O(2) $p_z$ ($a_{1g}$) |
| | | | | O(1) $p_\sigma$ ($a_{1g}$) |
| | | | | Cu $d_{3z^2-r^2}$ |
| (A) | 0.958 | −0.248 | −0.112 | |
| (B) | 0.959 | −0.246 | −0.128 | |
| (C) | 0.959 | −0.243 | −0.135 | |
| (D) | 0.959 | −0.241 | −0.143 | |

Figure 5.3: The CI wavefunctions of the $^1A_{1g}$ state in the $CuO_6$ cluster. The Cu–O(2) distance, $c$, is (A) 2.41Å, (B) 2.35Å, (C) 2.30Å and (D) 2.24Å, respectively. The atomic orbital with the largest component is attached to each MCSCF one-electron orbital in the right side.

with the original hole, as in a Heitler-London wavefunction. This situation corresponds to the spin-singlet coupling between Cu $d_{x^2-y^2}$ and O(1) $p_\sigma$ holes suggested by Zhang and Rice [60].

In the third configuration, the $a_{1g}$ orbital, $\psi_1$, is unoccupied while the $b_{1g}$ orbitals, $\psi_4$ and $\psi_5$, are doubly occupied. $\psi_1$, shown in Fig.5.4, consists almost entirely of Cu $d_{3z^2-r^2}$. This configuration appears for the following reason. When two holes are at a Cu site, the on-site Coulomb repulsion, the so-called Hubbard U, raises the energy. The Coulomb repulsion is smaller when the holes occupy both the $d_{3z^2-r^2}$ and the $d_{x^2-y^2}$ orbitals than when they remain only at the $d_{x^2-y^2}$ orbital. Thus the mixing of the $(d_{3z^2-r^2})^2$ and the $(d_{x^2-y^2})^2$ configurations reduces the Hubbard U at the Cu site, compared with the single configuration $(d_{x^2-y^2})^2$. The coefficient of the third configuration in the CI wavefunction becomes larger as Cu–O(2) distance decreases, as shown in Fig.5.3. This is because the energy levels of the $d_{x^2-y^2}$ and the $d_{3z^2-r^2}$ orbitals become closer as the $CuO_6$ geometry approaches a perfect octahedron.

The MCSCF one-electron orbitals change little when the Cu–O(2) distance is changed. $\psi_1$ still consists almost entirely of $d_{3z^2-r^2}$ orbital, although the components of the O(2) $p_z$



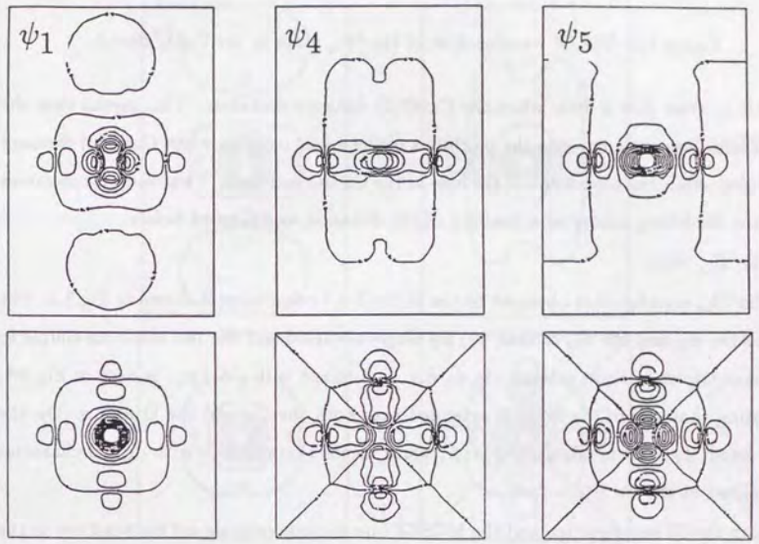


Figure 5.4: The MCSCF one-electron orbitals for the $^1A_{1g}$ state in the $CuO_6$ cluster ($c$ = 2.41Å). The upper row shows the wavefunctions perpendicular to the $CuO_2$ plane, the lower row shows the wavefunctions in the $CuO_2$ plane. The contour lines are drawn every 0.05.

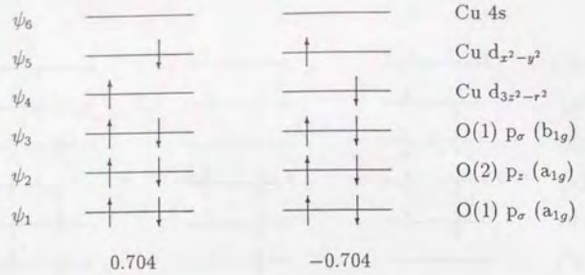


Figure 5.5: The CI wavefunction of the $^3B_{1g}$ state in the $CuO_6$ cluster.

orbitals increase just a little when the Cu–O(2) distance decreases. This means that the added hole does not enter into the p orbitals of the apical oxygens when Cu–O(2) distance is reduced, while the proportion of the hole at the Cu site increases. This result is consistent with the Madelung energy as a function of the distance, as discussed before.

(2) $^3B_{1g}$ State

The $^3B_{1g}$ wavefunction obtained by the MCSCF-CI calculation is shown in Fig.5.5. The $a_{1g}$ orbital, $\psi_4$, and the $b_{1g}$ orbital, $\psi_5$, are singly occupied and the two electrons couple to be a spin-triplet in these orbitals. In $\psi_5$ $d_{x^2-y^2}$ is mixed with O(1) $p_\sigma$, as seen in Fig.5.6, indicating that one of the holes is extended over both the Cu and the O atoms. On the other hand, $\psi_4$ consists mainly of $d_{3z^2-r^2}$, which means that one hole with $d_{3z^2-r^2}$ character is localized at the Cu site.

Both the CI wavefunction and the MCSCF one-electron orbitals are not sensitive to the Cu–O(2) distance in the $^3B_{1g}$ state.

The energy difference between the $^1A_{1g}$ and the $^3B_{1g}$ states is shown in Fig.5.7 as a function of the Cu–O(2) distance. As the apical O is closer to the $CuO_2$ plane, the energy difference decreases rapidly and at some distance the $^3B_{1g}$ state becomes stable. The reason for the conversion of the ground state from $^1A_{1g}$ to $^3B_{1g}$ is the following. When the Cu–O(2) distance decreases, the energy difference between the $b_{1g}$ orbital of Cu $d_{x^2-y^2}$ character and the $a_{1g}$ orbital of Cu $d_{3z^2-r^2}$ character becomes smaller, so that the energy of the $^3B_{1g}$ state is lowered, compared to that of the $^1A_{1g}$ state. The net effect is that the intra-atomic exchange interaction, the so-called Hund's coupling, favors a parallel spin configuration.



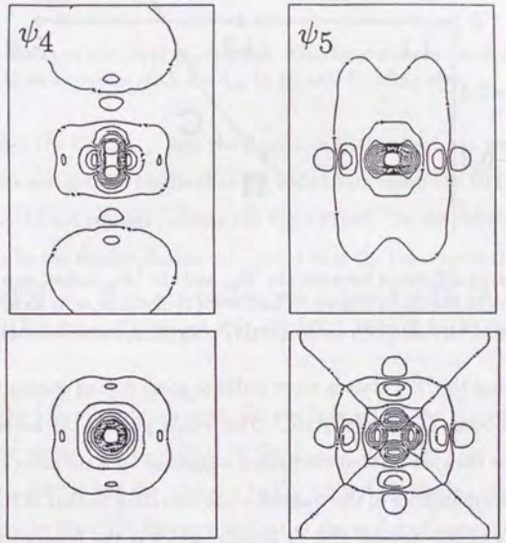


Figure 5.6: The MCSCF one-electron orbitals for the $^3B_{1g}$ state in the $CuO_6$ cluster ($c$ = 2.41Å). The upper row shows the wavefunctions perpendicular to the $CuO_2$ plane, the lower row shows the wavefunctions in the $CuO_2$ plane. The contour lines are drawn every 0.05.

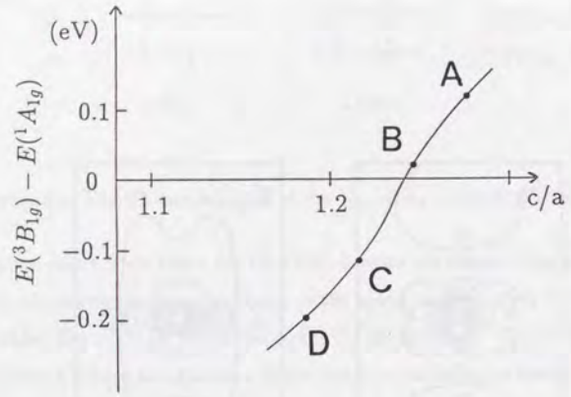


Figure 5.7: The energy difference between the $^3B_{1g}$ and the $^1A_{1g}$ states, as a function of the Cu–O(2) distance, $c$, in the $CuO_6$ cluster. The Cu–O(1) distance, $a$, is fixed at 1.889 Å. $c$ is 2.41Å(undoped case) (A), 2.35Å(B), 2.30Å (Sr-10% doped) (C) and 2.24Å(D), respectively.

This indicates that the $^3B_{1g}$ state is more stable at some doping concentration and that a transition should occur to a triplet state.[1] This would provide the necessary electronic configuration for the the spin polaron mechanism suggested by Kamimura *et al.* [61,62,63]. In addition, the correspondence of the transition concentration to that of the superconductivity transition [64,65,66], around 10% Sr doping, which is the interpolated value using the experimental results by Boyce *et al.*[50], is suggestive of the validity of the spin polaron model.

The strength of the Hund's coupling can be estimated directly from the energy difference between the $^3B_{1g}$ state and the excited $^1B_{1g}$ state. The estimated value is 2.0 eV.

(3) Other Symmetry States

Until now we have only considered the cases that the doped hole enters the oxygen $p_\sigma$ orbitals. But some people insist that the doped holes enter the oxygen $p_\pi$ orbitals which

[1]This transition has been also suggested by A.Fujimori [67]. However, his calculated result differs in two respects from ours. In his result the hole population at the apical oxygens is considerably large in the $^3B_{1g}$ state, while in our result the hole hardly enters the apical oxygen orbitals. In addition, the strength of the Hund's coupling is estimated to be about 0.05 eV in his calculation, while it is 2.0 eV in ours.



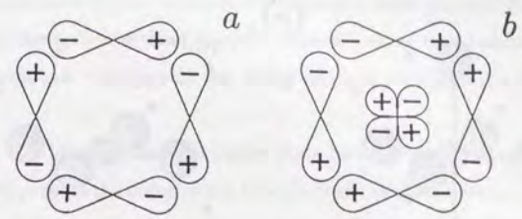


Figure 5.8: Two kinds of the O(1) $p_\pi$ orbitals. Orbital $a$ couples with none of the Cu d orbitals, while orbital $b$ couples with Cu $d_{xy}$ in an anti-bonding way.

couple with neither the Cu $d_{x^2-y^2}$ nor the $d_{3z^2-r^2}$ orbitals. Asai has performed *ab initio* cluster calculations and got the results that the added hole enters the O(1) $p_\pi$ orbital which couples with none of Cu d orbitals (orbital $a$ in Fig.5.8) [48]. On the other hand, Yamaguchi *et al.* have shown by the similar cluster calculation that the hole enters the O(1) $p_\pi$ orbital which couples with Cu $d_{xy}$ in an anti-bonding way (orbital $b$ in Fig.5.8) [47]. We perform the UHF calculations for the spin-triplet state so as to compare the energies among these states.

We consider the following three states: (1) one hole enters the $b_{1g}$ orbital of Cu $d_{x^2-y^2}$ character and one enters the $a_{1g}$ orbital of Cu $d_{3z^2-r^2}$ character (the $^3B_{1g}$ state studied above), (2) the $b_{1g}$ orbital and the orbital $a$ in Fig.5.8 and (3) the $b_{1g}$ orbital and orbital $b$ in Fig.5.8. We fix the Cu–O(2) distance at that of the undoped compound. The energies of these states are (1) 0.14 eV (2) 1.3 eV and (3) 1.7 eV, measured from the $^1A_{1g}$ state energy calculated using the MCSCF-CI method. Hence state (1) is the most stable among them.

The different results of similar cluster calculations by the other groups seem to be due to the different selection of the oxygen's basis set. We don't use the diffuse components for $O^{2-}$ while the other groups have used them. In their calculated results, therefore, the $p_\pi$ orbitals overlap well with each other and a hole in the orbitals obtains a lower kinetic energy, compared with in our calculation. In their calculations, however, the diffuse components cause problems with the point charge approximation outside of the cluster, because the diffuse components reach the nearest neighbor sites with considerable amplitudes. In

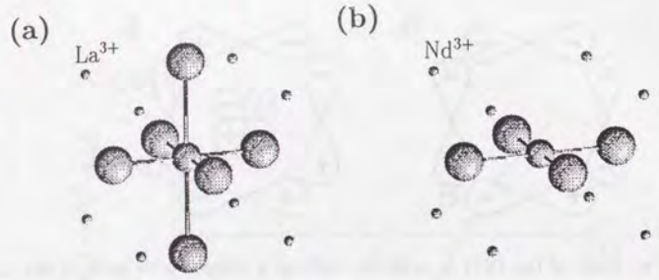


Figure 5.9: (a) $CuO_6$ and (b) $CuO_4$ clusters with the nearest neighboring trivalent ions.

addition, if the doped hole occupies the O $p_\pi$ orbital, we will not be able to explain the observed fact that the anti-ferromagnetic ordering of the Cu spins disappears by the hole doping.

Although the shape of the oxygen $p_\pi$ orbitals depends well on the basis set, that of the oxygen $p_\sigma$ orbitals is not essentially affected by the basis set, since in these orbitals the diffuse components of the O atoms are not important, owing to the existence of the Cu $d_{x^2-y^2}$ or $d_{3z^2-r^2}$ basis functions. Our calculated results about the $^1A_{1g}$ and $^3B_{1g}$ states, therefore, will be little changed by adopting the diffuse components.

### 5.3.3 Effect of the Doped $Sr^{2+}$ Ions

In this subsection we investigate the effect of doped $Sr^{2+}$ ions in the $La_{2-x}Sr_xCuO_4$ compound, where the $Sr^{2+}$ ions are substituted for the $La^{3+}$ ions. For this purpose we change the point charges outside the cluster in the two following ways: (i) We replace all of the eight +3e charges, which are the nearest $La^{3+}$ sites to the cluster, by +2.875e point charges. (ii) We replace only one of the eight +3e by a +2e point charge (see Fig.5.9 (a)). Then we consider the electrically neutral hole-doped systems. The Cu–O(2) distance is fixed at the value of the undoped case.

In situation (i) we perform independent MCSCF-CI calculations for the $^1A_{1g}$ and the $^3B_{1g}$ states. The many-body wavefunctions and the MCSCF one-electron orbitals are almost the same as before. Although the $^1A_{1g}$ state is energetically more stable than the



$^3B_{1g}$ state, the energy difference between these states is much reduced, down to 0.046 eV from 0.117 eV in the system without the $Sr^{2+}$. This is because the Madelung energy at the O(2) site decreases and consequently the energy of the $a_{1g}$ orbital of Cu $d_{3z^2-r^2}$ character is increased.

In situation (ii), however, the spin-triplet state becomes unstable, compared with the singlet state. We perform the unrestricted Hartree-Fock calculation for the spin-triplet state and the restricted Hartree-Fock for the singlet state. The energy of the spin-triplet state is higher by 7.7 eV than that of the singlet state, with RHF for both states this difference is increased. This is because the $D_{4h}$ symmetry is broken so that the energy difference between the Cu $d_{x^2-y^2}$ and $d_{3z^2-r^2}$ orbitals becomes large, as a result, the Hund's coupling becomes less effective. If we include further the correlation energy which is not included in the HF calculation, the energy difference between the spin-singlet and the triplet states becomes larger since the correlation effect is larger in the spin-singlet state. This lowers the spin-singlet state's energy, and the spin-triplet state, therefore, becomes more unstable with respect to it.

We conclude that there are two kinds of effects of the doped $Sr^{2+}$ ions, one favoring the spin-triplet state and the other opposing it. If the doped divalent ions influence the electronic state in a random, averaged way, the triplet state becomes stable. On the other hand, if the randomness affects the electronic state locally, the triplet state becomes unstable, owing to the broken spatial symmetry.

## 5.4 $CuO_4$ Cluster

In this section we describe the electronic structure in the $CuO_4$ cluster for the Nd-Cu-O system.

### 5.4.1 Undoped System

We perform the UHF calculation for the spin-doublet state in the undoped $CuO_4$ cluster. The Cu $d_{x^2-y^2}$–O $p_\sigma$ anti-bonding $b_{1g}$ orbital is singly-occupied. Compared to the $CuO_6$ cluster, the component of O $p_\sigma$ is smaller in the orbital and thus the covalency between Cu and O is smaller in this system. The Mulliken charges, which are listed in Table 5.3,

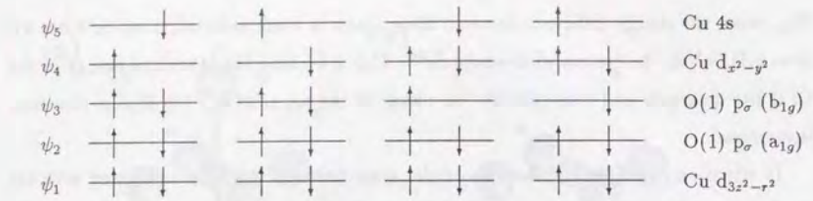


| | | | | |
|---|---|---|---|---|
| (g) | 0.686 | −0.686 | −0.168 | 0.168 |
| (ex) | 0.687 | 0.687 | 0.166 | 0.166 |

Figure 5.10: The CI wavefunctions of the ground state ($^3B_{1g}$) and the first excited state ($^1B_{1g}$) in the $CuO_4$ cluster.

also indicate that the ionicity is stronger in $Nd_2CuO_4$ than in $La_2CuO_4$. The ionicity of $Nd_2CuO_4$ is almost the same as that of NiO. This stronger ionicity in $Nd_2CuO_4$ is due to the fact that the Cu–O(1) distance is longer in $Nd_2CuO_4$ than in $La_2CuO_4$.

### 5.4.2 Electron-doped System

When an electron is added to the undoped $CuO_4$ cluster, there are two possibilities of the electronic state. (i) The electron enters the $b_{1g}$ orbital of Cu $d_{x^2-y^2}$ character ($^1A_{1g}$ state). (ii) The electron enters the $a_{1g}$ orbital of Cu 4s character ($^3B_{1g}$ state). Then we perform the MCSCF-CI calculations for both states independently, as in the previous section.

As all our calculations give the $^3B_{1g}$ state as the ground state in this system, we present the calculated results for the $^3B_{1g}$ state only.

The many-body wavefunctions of the ground and the first excited states are given in Fig.5.10. The MCSCF one-electron orbitals are shown in Fig.5.11. The ground state consists mainly of four configurations. In the first two configurations, which have the largest coefficients, the $b_{1g}$ orbital $\psi_4$ and the $a_{1g}$ orbital $\psi_5$ are singly occupied and two electrons make a spin-triplet coupling in these orbitals. $\psi_4$ is almost completely Cu $d_{x^2-y^2}$ in character, while $\psi_5$ consists mainly of Cu 4s, as seen in Fig.5.11. In the last two configurations the singly occupied orbitals are $\psi_4$ and $\psi_3$. $\psi_3$ consists mainly of the O $p_\sigma$ orbital with $b_{1g}$ symmetry. This indicates that an added electron enters the Cu 4s and couples ferromagnetically with an electron in the $b_{1g}$ orbital.



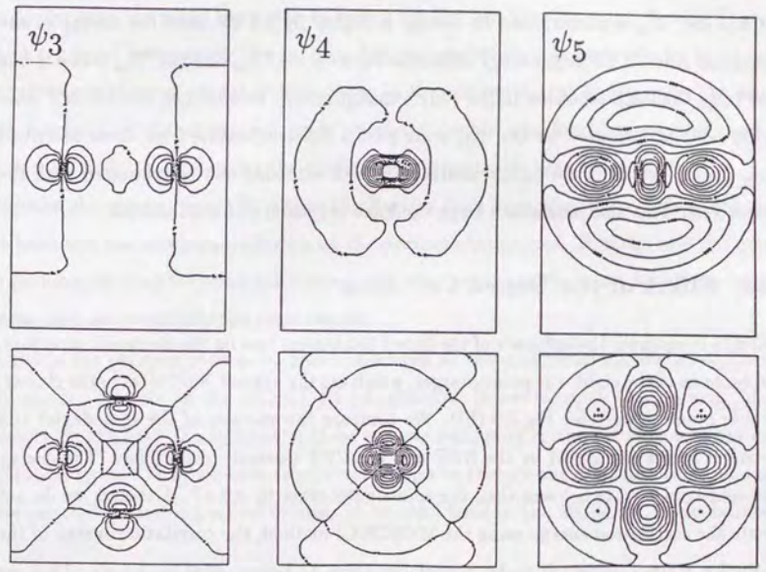


Figure 5.11: The MCSCF one-electron orbitals for the $^3B_{1g}$ state in the $CuO_4$ cluster. The upper row shows the wavefunctions perpendicular to the $CuO_2$ plane, the lower row shows the wavefunctions in the $CuO_2$ plane. The contour lines are drawn every 0.05 for $\psi_3$ and $\psi_4$, every 0.01 for $\psi_5$.

In the first excited state two electrons make a spin-singlet pair in the $\psi_4$ and the $\psi_5$ orbitals, or in the $\psi_3$ and the $\psi_5$ orbitals ($^1B_{1g}$ state). The excitation energy is 0.05 eV. Thus the strength of the Hund's coupling is much weaker than that in the hole-doped $CuO_6$ cluster. This is because the exchange integral between the Cu $d_{x^2-y^2}$ and 4s orbitals is much smaller than that between the Cu $d_{x^2-y^2}$ and $d_{3z^2-r^2}$ orbitals. The second excited state has the $^1A_{1g}$ symmetry and its energy is higher by 1.1 eV than the energy of the $^3B_{1g}$ ground state. This large energy difference between the $^1A_{1g}$ and the $^3B_{1g}$ states is due to the large Coulomb repulsion in the $(3d)^{10}$ configuration. In addition, the MCSCF one-electron orbitals optimized for the $^1A_{1g}$ state have a different feature from those described before; the $a_{1g}$ orbital of Cu $d_{3z^2-r^2}$ character is well extended and is hybridized with the Cu 4s orbital. This also indicates a large Coulomb repulsion in Cu 3d orbital.

### 5.4.3 Effect of the Doped $Ce^{4+}$ Ions

In order to investigate the influence of the doped tetravalent ions on the electronic structure, we replace one of the eight +3e point charges, which are the nearest $Nd^{3+}$ sites to the cluster, by a +4e point charge (see Fig.5.9 (b)). We compare the energies of the spin-singlet and spin-triplet states calculated by the RHF and the UHF method, respectively. The energy of the spin-triplet state is lower than the spin-singlet state by 4.5 eV. Although we do not evaluate the correlation energy using the MCSCF-CI method, the correlation energy of the spin-singlet state is expected to be almost the same as before, that is, 3.6 eV. Thus we conclude that the spin-triplet state is still stable in this system, in contrast to the hole-doped $CuO_6$ cluster. This is because the spin-triplet state is stable in the electron-doped $CuO_4$ cluster, owing to the large Coulomb repulsion in the $(3d)^{10}$ configuration, which is not affected by breaking the $D_{4h}$ symmetry.

This result indicates that the spin-triplet state is qualitatively different between the electron-doped Nd-Cu-O system and the hole-doped La-Cu-O system. In the former an electron enters the Cu 4s orbital to avoid the strong repulsive energy of the 3d orbitals, and make a weak spin-triplet pair with a spin in the 3d orbital. On the other hand, the triplet state in the La-Cu-O system arises due to the occurrence of two nearly degenerate levels, and thus the geometrical symmetry is essentially important.



## 5.5 $Cu_2O_{11}$ and $Cu_2O_7$ Clusters

In this section we present the electronic structures of the $Cu_2O_{11}$ and the $Cu_2O_7$ clusters. The calculations are done in almost the same way as for the $CuO_6$ and the $CuO_4$ clusters, although the following two points are different.

(i) We take the same basis sets as before for the two Cu atoms and for the O atom which is placed between the two coppers, but we take single zeta basis sets for 1s, 2s and 2p orbitals of the rest oxygen atoms, owing to the computational limitations. The single zeta functions of the oxygen are made up of the double zeta functions we have used in section 5.3 and 5.4, by keeping the coefficients of the double zeta functions fixed so as to minimize the energy of an $O^{2-}$ ion in the Hartree-Fock approximation. This selection of the basis sets has no serious influence on the electronic structures. To make sure this point, we perform the $Cu_2O_7$ cluster calculation with the double zeta basis set for all the oxygen atoms, and get essentially the same results.

(ii) In the previous section we have considered all the configurations, including the $a_{1g}$ and the $b_{1g}$ orbitals, in the MCSCF-CI calculations. However, since $Cu_2O_{11}$ and $Cu_2O_7$ clusters do not have $D_{4h}$ symmetry, there is some ambiguity in the restriction of the configuration space. Thus we have tried several ways to restrict the configuration space and have selected several important orbitals to be considered in the MCSCF-CI calculations.

### 5.5.1 Undoped Systems

In the undoped $Cu_2O_{11}$ cluster, the ground state is a spin-singlet owing to the superexchange between two spins at Cu sites, while the first excited state is a spin-triplet. Thus we perform the MCSCF-CI calculations for both the spin-singlet and the spin-triplet states. As we get almost the same optimized MCSCF one-electron orbitals for both states, we perform all the CI calculations based on the MCSCF orbitals optimized for the spin-singlet state.

The many-body wavefunctions of the ground and the first excited states are given in Fig.5.12. The spatial distributions of the MCSCF one-electron orbitals are shown in Fig.5.13, indicating that $\psi_2$ and $\psi_3$ correspond, respectively, to the bonding and the anti-

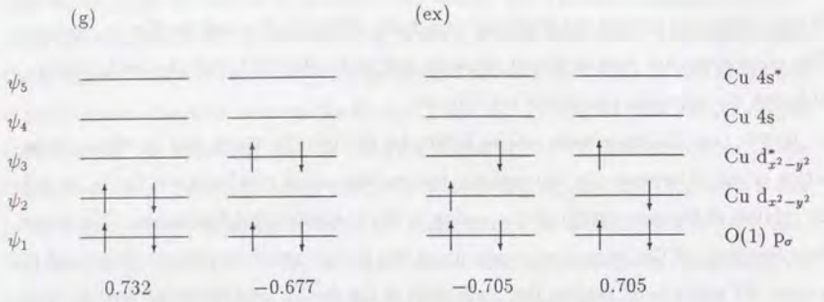


Figure 5.12: The CI wavefunctions of the ground state and the first excited state in the undoped $Cu_2O_{11}$ cluster.

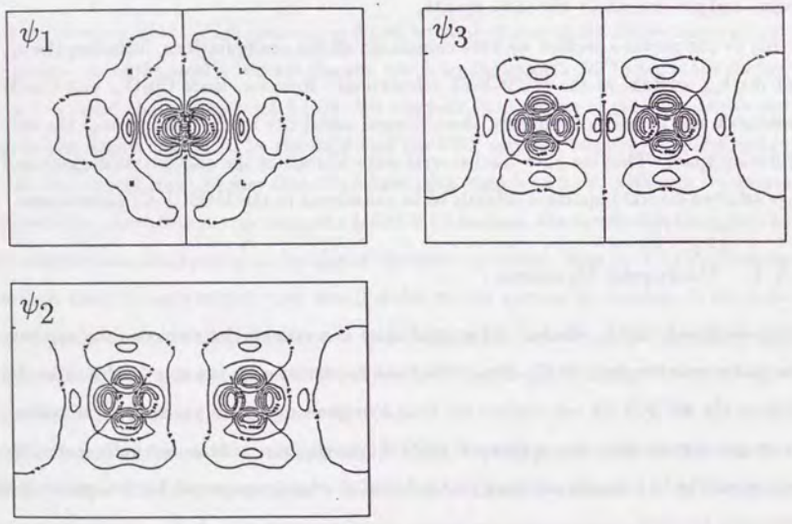


Figure 5.13: The MCSCF one-electron orbitals in the undoped $Cu_2O_{11}$ cluster. The wavefunctions in the $CuO_2$ plane are shown. The contour lines are drawn every 0.04.



bonding orbitals between the two Cu $d_{x^2-y^2}$ orbitals. These orbitals also include small amplitudes of the O $p_\sigma$ orbitals, which are hybridized with the Cu $d_{x^2-y^2}$ orbitals in an anti-bonding way. As seen in Fig.5.12, the ground state is a spin-singlet, and consists of two configurations in which one of $\psi_2$ or $\psi_3$ is doubly-occupied, like in a Heitler-London wavefunction. This indicates that the two electrons are localized at the Cu $d_{x^2-y^2}$ orbitals and that they are coupled anti-ferromagnetically. The two electrons are coupled ferromagnetically in these orbitals in the first excited state. From the excitation energy to the first excited state, we can estimate the value of the exchange integral, $J$, in the Heisenberg Hamiltonian, $H_{ex} = J \sum_{(i>j)} \mathbf{S}_i \cdot \mathbf{S}_j$, between two electrons in neighboring Cu $d_{x^2-y^2}$ orbitals. This is found to be 360 K, which corresponds to only about a fifth of the experimental result, $J = 1600$K, for the $La_2CuO_4$ compound [68,69].

The electronic structure in the undoped $Cu_2O_7$ cluster is very similar to that in the $Cu_2O_{11}$ cluster. The wavefunctions of the ground and the first excited states are shown in Fig.5.14. The MCSCF one-electron orbitals are presented in Fig.5.15. In the ground state two electrons form a spin-singlet pair in the orbitals $\psi_2$ and $\psi_3$, while in the first excited state they form a spin-triplet pair in these orbitals. $\psi_2$ and $\psi_3$ are bonding and anti-bonding orbitals between the two Cu $d_{x^2-y^2}$ orbitals. The O $p_\sigma$ contribution is smaller in the $Cu_2O_7$ cluster than in the $Cu_2O_{11}$ cluster. The value of the exchange integral $J$ is estimated to be 260 K,[1] which is also much smaller than the experimental value 1400 K for the $Nd_2CuO_4$ compound [70,71].

The calculated values of the exchange integral $J$ are smaller than those of the experimental results for both the $La_2CuO_4$ and the $Nd_2CuO_4$ compounds. This disagreement with the experiments may be ascribed to finite size effects of the clusters. The anti-ferromagnetic exchange is due to the superexchange mechanism through which an oxygen atom mediates between the two Cu atoms. The mechanism includes the virtual process in which an electron moves from the O $p_\sigma$ orbital to the Cu $d_{x^2-y^2}$ orbitals, that is, $Cu^+$ and $O^-$ states appear. In the larger system this virtual state may be stabilized by the relaxation of the electronic configuration around the $Cu^+$–$O^-$ sites. In our cluster calculations, however, this

[1] When we perform the $Cu_2O_7$ cluster calculation with the double zeta basis sets for all the oxygen atoms, the value of $J$ is estimated to be 270 K.

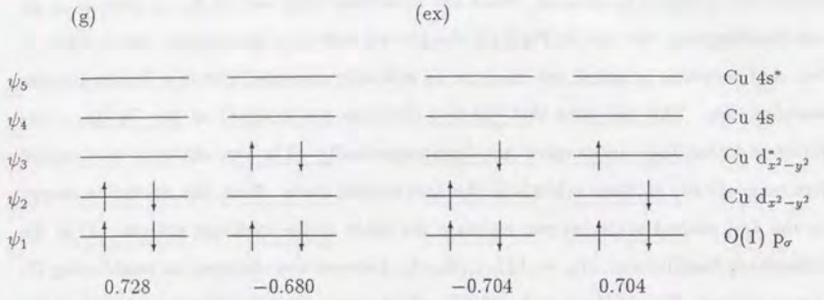


Figure 5.14: The CI wavefunctions of the ground state and the first excited state in the undoped $Cu_2O_7$ cluster.

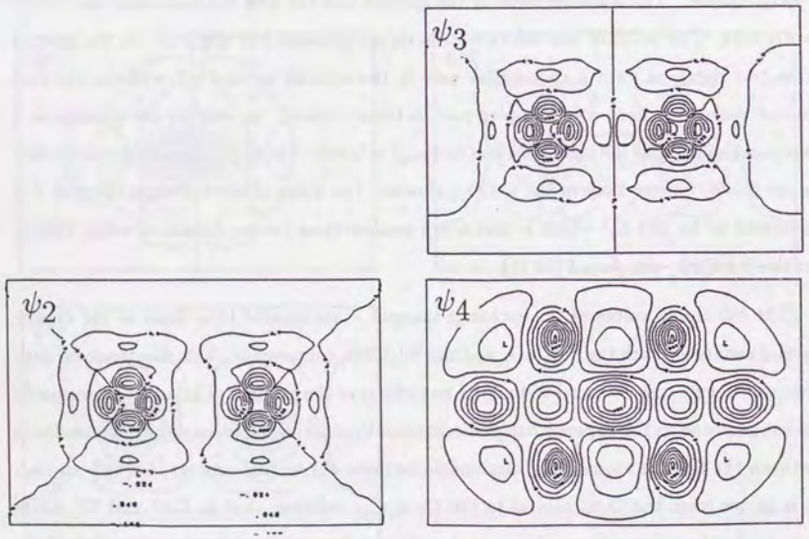


Figure 5.15: The MCSCF one-electron orbitals in the undoped $Cu_2O_7$ cluster. The wavefunctions in the $CuO_2$ plane are shown. The contour lines are drawn every 0.04 for $\psi_2$ and $\psi_3$, every 0.01 for $\psi_4$.



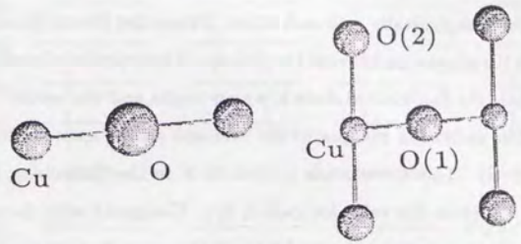


Figure 5.16: $Cu_2O$ and $Cu_2O_5$ clusters. We perform the calculations of these two clusters for $La_2CuO_4$, and the calculation of the $Cu_2O$ cluster for $Nd_2CuO_4$.

| | $Cu_2O_{11}$ ($Cu_2O_7$) | $Cu_2O_5$ | $Cu_2O$ |
|---|---|---|---|
| $La_2CuO_4$ | 360K | 150K | 97K |
| $Nd_2CuO_4$ | 260K | | 110K |

Table 5.4: The calculated values of the exchange integral between Cu spins, $J$, in the $Cu_2O_{11}$ ($Cu_2O_7$), $Cu_2O_5$ and $Cu_2O$ clusters.

effect is not enough taken into account and, as a result, the virtual process is suppressed and the superexchange effect becomes smaller.

To investigate the mechanism mentioned above further, we carry out the MCSCF-CI calculations for the smaller clusters; $Cu_2O$, $Cu_2O_5$ for $La_2CuO_4$ and $Cu_2O$ for $Nd_2CuO_4$ (see Fig.5.16). The point charges are placed outside of the clusters in the same way as before. The values of the calculated exchange integral, $J$, between the Cu spins are listed in Table 5.4. As the number of oxygen atoms around a Cu site decreases, the value of $J$ becomes smaller. This result indicates the importance of the relaxation effect and the covalent effect around the Cu sites in the mechanism of the superexchange.

In comparison, we perform the MCSCF-CI calculation of the $Ni_2O_{11}$ cluster for NiO. It should be noted that the two Ni atoms in the cluster are not nearest neighbors but second nearest neighbors. We consider the two nearest Ni sites, which belong to the different magnetic sublattices in the anti-ferromagnetic ordering of the NiO crystal [12], in order to investigate the superexchange mechanism through the oxygen between them.

In NiO each Ni site has a triplet spin, as seen in section 5.3.1, and the two pairs of spin-triplet couple anti-ferromagnetically with each other. This is also due to the superexchange mechanism through the oxygen ion between the Ni ions. In the calculated result, the ground state is a spin-singlet, the first excited state is a spin-triplet and the second excited state has total spin 2. The excitation energies to the first and second excited states are 79 K and 237 K, respectively. This corresponds to $J = 79$ K in the Heisenberg Hamiltonian, $H_{ex} = J \sum_{(i>j)} \mathbf{S}_i \cdot \mathbf{S}_j$, where the value for each $\mathbf{S}_i$ is 1. Compared with the experimental value of 210 K [72], this calculation is better for the NiO system than for the $La_2CuO_4$ and $Nd_2CuO_4$ systems.

As seen before, ionicity is stronger in NiO than in $La_2CuO_4$. Thus the finite size effect is expected to be smaller for NiO. In $La_2CuO_4$ the covalent character between the Cu and the O(1) atoms plays an important role, consequently the finite size effect becomes more serious in the mechanism of the superexchange. In addition, the difference in the crystal structures may also play a role. This would account for the poor agreement of $J$ with experiment in the $Nd_2CuO_4$ case, despite it having a similar ionicity to NiO. In particular, there are oxygen lone pair electrons in the $La_2CuO_4$ and the $Nd_2CuO_4$ compounds, which are able to relax easily.

### 5.5.2 Hole-Doped $Cu_2O_{11}$

Now we proceed to discuss the hole-doped $Cu_2O_{11}$ cluster. For simplicity, we perform the CI calculation, using the MCSCF one-electron orbitals optimized for the spin-singlet state of the undoped $Cu_2O_{11}$ system (see Fig.5.13).

The many-body wavefunctions of the ground and the first excited states are shown in Fig.5.17. The ground state is a spin-doublet and consists mainly of four configurations. In the first configuration the $\psi_2$ orbital is singly-occupied, that is, one electron is in the Cu $d_{x^2-y^2}$ orbitals. In the other three configurations the $\psi_1$, $\psi_2$ and $\psi_3$ orbitals are singly-occupied. Thus a hole enters the $\psi_1$ orbital, which corresponds to the $p_\sigma$ orbital of the central oxygen. The contribution of the first configuration is 38%, while the total contribution of the latter three is 59%. Using Clebsch-Gordan coefficients, we can transform the latter three configurations into two parts, one includes the spin-triplet coupling of two



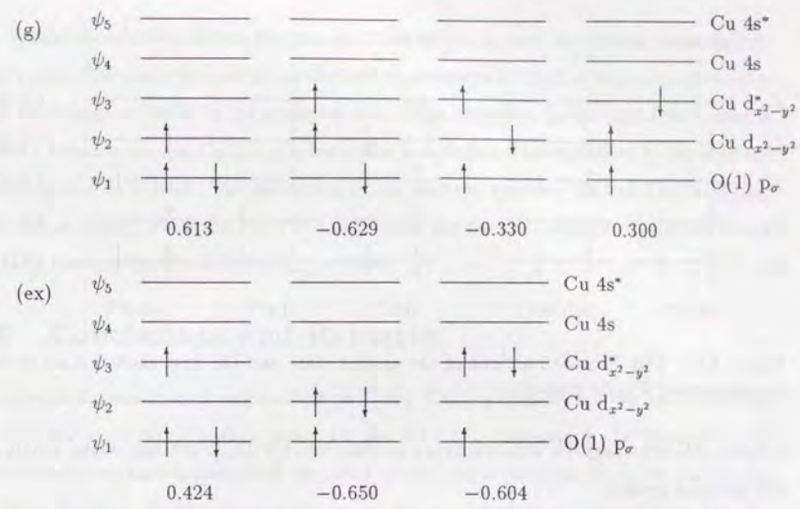


Figure 5.17: The CI wavefunctions of the ground state and the first excited state in the hole-doped $Cu_2O_{11}$ cluster. Only main configurations are listed.

electrons in the $\psi_2$ and the $\psi_3$ orbitals, $|(s_1 = \frac{1}{2}, S_{2,3} = 1)S_{total} = \frac{1}{2}\rangle$, the other includes the singlet coupling between them, $|(s_1 = \frac{1}{2}, S_{2,3} = 0)S_{total} = \frac{1}{2}\rangle$, as

$$0.77|(s_1 = \frac{1}{2}, S_{2,3} = 1)S_{total} = \frac{1}{2}\rangle + 0.023|(s_1 = \frac{1}{2}, S_{2,3} = 0)S_{total} = \frac{1}{2}\rangle.$$

This indicates that the spin coupling of the two Cu sites is almost entirely ferromagnetic, $S_{2,3} = 1$ component, (more than 99%) when the added hole occupies the O(1) $p_\sigma$ orbital. This is the result of an anti-ferromagnetic direct exchange between the Cu and the O(1) unpaired spins.

The first excited state is also a spin-doublet and consists mainly of three configurations. In the first configuration the $\psi_3$ orbital, which consists almost entirely of the two Cu $d_{x^2-y^2}$ orbitals, is singly-occupied. In the rest two configurations the $\psi_1$ accommodates one hole, and two electrons couple anti-ferromagnetically in $\psi_2$ and $\psi_3$, like in a Heitler-London wavefunction. The excitation energy to the first excited state is 1.13eV, which is much larger than that in the undoped system, 0.031eV. This is because the direct exchange between the O $p_\sigma$ and the Cu $d_{x^2-y^2}$ orbitals is strong in the hole doped system, while the

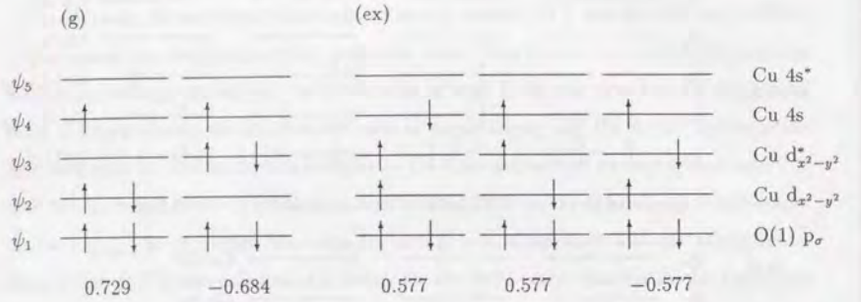


Figure 5.18: The CI wavefunctions of the ground state and the first excited state in the electron-doped $Cu_2O_7$ cluster.

indirect anti-ferromagnetic superexchange between two Cu $d_{x^2-y^2}$ orbitals works weakly in the undoped system.

In the $Cu_2O_{11}$ cluster the symmetry of the Cu site is lower than that in the $CuO_6$ cluster and also that in the elongated octahedral La-Cu-O system. Thus the energy difference between the Cu $d_{x^2-y^2}$ and $d_{3z^2-r^2}$ orbitals is larger, so that the holes hardly occupy the $d_{3z^2-r^2}$ orbitals. This is in contrast to the situation in the $CuO_6$ cluster, mentioned before.

### 5.5.3 Electron-Doped $Cu_2O_7$

In this subsection we present the investigation of the electron-doped $Cu_2O_7$ cluster. We perform the CI calculation, based on the MCSCF one-electron orbitals, shown in Fig.5.15, optimized for the undoped $Cu_2O_7$ system.

The many-body wavefunctions of the ground and the first excited states are shown in Fig.5.18. The ground state is a spin-doublet, in which the bonding orbital between the two Cu 4s, $\psi_4$, is singly-occupied. Two electrons exhibit a spin-singlet coupling in the $\psi_2$ and the $\psi_3$ orbitals. The occupation ratio of the two Cu $d_{x^2-y^2}$ bonding orbital ($\psi_2$) to the anti-bonding orbital ($\psi_3$) is almost the same as in the ground state of the undoped case (see Fig.5.14). This indicates that the electronic state in the Cu $d_{x^2-y^2}$ orbitals does not change while the doped electron is added to the 4s orbitals.

In the first excited state, the three electrons couple to the spin-quartet state in the



$\psi_2$, $\psi_3$ and $\psi_4$ orbitals. Hence the two electrons in the $\psi_2$ and $\psi_3$ orbitals make a spin-triplet pair. The excitation energy to the first excited state is 120K, which is much smaller than the energy of 260K in the undoped case. This reduction in the anti-ferromagnetic coupling between the two Cu $d_{x^2-y^2}$ spins is due to a double exchange effect by the electron occupying the $\psi_4$ orbital. The movement of the electron between the two Cu 4s orbitals reduces the energy when the two Cu $d_{x^2-y^2}$ spins are parallel, owing to the Hund's rule coupling between the Cu 4s and $d_{x^2-y^2}$ orbitals.

## 5.6 Conclusions and Remarks

We have performed cluster calculations on $CuO_6$, $Cu_2O_{11}$ clusters for the La-Cu-O compounds, and on $CuO_4$, $Cu_2O_7$ clusters for the Nd-Cu-O compounds. In the hole-doped $CuO_6$ cluster we have investigated the effect of the apical oxygens, O(2), by varying the Cu–O(2) distance. As the distance decreases, the ground state is changed from the $^1A_{1g}$ state to the $^3B_{1g}$ state at some Cu–apical O distance, which corresponds to the value of about 10% Sr doped compound. The $^3B_{1g}$ state becomes more stable, if the effect of the doped divalent ions is in a randomly averaged way. In the $^1A_{1g}$ state the contribution of the Cu $d_{3z^2-r^2}$ orbital to the wavefunction increases to reduce the Hubbard U at the Cu site, with decreasing Cu–O(2) distance. These both show the importance of the decrease in the energy difference between the Cu $d_{x^2-y^2}$ and the $d_{3z^2-r^2}$ orbitals, as the Cu–O(2) distance is reduced. In the electron-doped $CuO_4$ cluster the ground state has the $^3B_{1g}$ symmetry, in which both the Cu 4s and the $3d_{x^2-y^2}$ orbitals are singly-occupied.

In the undoped $Cu_2O_{11}$ and $Cu_2O_7$ clusters, the two electrons couple anti-ferromagnetically in the two Cu $d_{x^2-y^2}$ orbitals. However, the calculated values of the exchange integral, $J$, are smaller than those of the experimental results. This may be due to the neglect of the relaxation effect outside the clusters. This effect seems more important in $La_2CuO_4$ and $Nd_2CuO_4$, than in NiO. When a hole is added to the $Cu_2O_{11}$ cluster, it mainly enters the $p_\sigma$ orbital of the central oxygen and the coupling of the two Cu $d_{x^2-y^2}$ spins changes to be ferromagnetic. When an electron is added to the $Cu_2O_7$ cluster, it occupies the Cu 4s orbitals and the coupling of the two Cu $d_{x^2-y^2}$ spins is still anti-ferromagnetic, although its coupling is weaken by the double exchange effect of the electron in the Cu 4s orbitals.

The added electron enters the Cu 4s orbital in the Nd-Cu-O system, according to the calculated results of both the $CuO_4$ and the $Cu_2O_7$ clusters. Thus we conclude that electrons can be doped to the Cu 4s orbitals in systems without apical oxygens, because their energy is lower, compared to that in the octahedron or pyramid structures.

As for hole doping in the La-Cu-O system, however, we have obtained results different for the $CuO_6$ and for the $Cu_2O_{11}$ clusters. In the former, both the Cu $d_{x^2-y^2}$ and the $d_{3z^2-r^2}$ orbitals play important roles, while in the latter, the hole hardly enters the Cu $d_{3z^2-r^2}$ orbitals but goes into the central O $p_\sigma$ orbital to gain the energy due to the direct exchange with two Cu spins. As a result, the hole is localized at the O site and the two Cu spins couple ferromagnetically in the ground state of the hole-doped $Cu_2O_{11}$ cluster. However, if this situation happens in the $CuO_2$ network of the La-Cu-O system, the kinetic energy of the hole is increased owing to its localized nature, and the spin states are frustrated, because the exchange interactions with the Cu spins surrounding the $Cu_2O_{11}$ cluster must be anti-ferromagnetic. In order to remedy this unrealistic situation, we should take account of the effect of the motion of the holes to regions outside of the cluster, so that the correct symmetry at the Cu site is restored as well as the kinetic energy effect is reduced. On the other hand, in the case of the $CuO_6$ cluster, the Cu site has the same symmetry, $D_{4h}$, as that in the bulk La-Cu-O system. Thus we expect that the calculated results of the $CuO_6$ cluster reflect the local properties of the electronic structure in the hole-doped bulk system correctly.



# Chapter 6

# Summary

In this chapter we summarize the results obtained and discuss the problems in our calculations.

In this thesis we have performed first principles investigations of two strongly correlated systems; the Anderson-localized states in the uncompensated and the compensated Si:P and the copper oxide materials of the high temperature superconductors. To take into account the correlation effect explicitly, we have adopted the MCSCF method in finite-size cluster models. In the MCSCF method one-electron orbitals are determined including a part of the correlation effect as well as the Coulomb and the exchange interactions. Hence we can get a clear cut view of the strongly correlated many-body states, by a small number of configurations, using the MCSCF orbitals as a basis set.

For the Anderson-localized states of the doped semiconductors, we have taken the cluster models in which donors (and acceptors) are distributed randomly. In the uncompensated Si:P system, the pair-type correlation effect is important between the localized electrons. This is the situation of the spin pair model, which holds even near the critical donor concentration of the MI transition, although the spin pairs are extended and overlap well each other. We have found that 10 to 20% of the spin pairs are spin-triplet, which may be attributed to the appearance of two nearly degenerate orbitals. In the compensated Si:P system, the MCSCF one-electron orbitals are more extended in space than those in the uncompensated case, and screen better the electron-electron interactions. Consequently the pair-type correlation effect is not so strong as in the uncompensated case. We have calculated the specific heat in the magnetic field and the spin-susceptibility, and explained

their temperature dependence.

As the donor concentration increases, the MCSCF one-electron orbitals become more extended, and the electron correlation becomes smaller owing to the stronger screening effect by the more extended MCSCF orbitals. This is the feature of the Mott-type MI transition. With increasing donor concentration, however, the finite size effect of the clusters may become serious. To investigate the electronic structure near the MI transition point further, we must perform the calculations of larger clusters. By this we may study the cluster size dependence of the electronic structure, or explore its scaling behavior. However, we think that the local properties of the electronic states can be described in this cluster simulation. We have already carried out the calculations of the 12-donor clusters and got qualitatively the same results.

In the copper oxide materials of the high temperature superconductors, we have adopted clusters of $CuO_6$, $Cu_2O_{11}$ and $CuO_4$, $Cu_2O_7$ for the $La_{2-x}Sr_xCuO_4$ and the $Nd_{2-x}Ce_xCuO_4$ compounds, respectively. In the hole-doped $CuO_6$ cluster, the Cu $d_{3z^2-r^2}$ orbital plays an important role as well as the $d_{x^2-y^2}$ orbital. As the Cu–apical O distance decreases, the ground state is changed from the $^1A_{1g}$ state to the $^3B_{1g}$ state. In addition, in the $^1A_{1g}$ state the contribution of the Cu $d_{3z^2-r^2}$ orbital increases to reduce the Hubbard U at the Cu site, with decreasing Cu–apical O distance. In the electron-doped $CuO_4$ cluster the added electron occupies the Cu 4s orbital ($^3B_{1g}$ state). In the undoped $Cu_2O_{11}$ and $Cu_2O_7$ clusters, the two electrons, which are localized at the Cu $d_{x^2-y^2}$ orbitals, couple anti-ferromagnetically, although the calculated values of the exchange integral, $J$, are not in agreement with the experimental values. This is due to the superexchange mechanism through the oxygen between the Cu atoms.

In the cluster calculations, however, we have neglected the periodicity of the crystals, although we have considered a part of the ions' effect outside of the cluster by including point charges. This approximation seems to be valid in the undoped clusters because the undoped compounds are anti-ferromagnetic insulators, and the electrons are localized at the Cu sites. When we consider the carrier-doped cases, finite size effects become serious. We should take account of the motion of the carriers to elucidate the electronic structures in the carrier-doped systems. Monte Carlo simulation may be a method suitable for this



purpose. However, we believe that the local properties and the correlation effect can be described qualitatively in our cluster calculations.

Our first principles calculation formalism is applicable to other strongly correlated electronic systems. By investigating other systems, we will understand the correlation effect on electronic structures further.

# Bibliography


[1] For a review, see *Electron-Electron Interactions in Disordered Systems*, eds. A.L.Efros and M.Pollak (North-Holland, Amsterdam, 1985).

[2] H.Kamimura, H.Aoki: International series of monographs on physics, Vol. 76, *The Physics of Interacting Electrons in Disordered Systems* (Clarendon press, Oxford, 1989).

[3] For a review, see *Theory of Heavy Fermions and Valence Fluctuations*, eds. T.Kasuya and T.Saso (Springer, Berlin, 1985).

[4] J.G.Bednorz and K.A.Müller: Z. Phys. **B64** (1986) 189.

[5] H. Shiba and M. Ogata: in Springer Series in Materials Science, Vol.11, *Mechanisms of High temperature Superconductivity*, eds. H.Kamimura and A.Oshiyama (Springer, Heidelberg, 1989) p. 44 and related references therein.

[6] M. Imada: J. Phys. Soc. Jpn. **57** (1988) 3128; in the same book as in Ref.[5], p. 53 and related references therein.

[7] For example, J.Callaway and N.H.March: *Density Functional Methods: Theory and Application*, in Solid State Physics, Vol. 38 (Academic Press, 1984) p.135.

[8] L.F.Mattheiss: Phys. Rev. Lett. **58** (1987) 1028.

[9] J.Yu, A.J.Freeman and J.H.Xu: Phys. Rev. Lett. **58** (1987) 1035.

[10] K. Shiraishi, A. Oshiyama, N. Sima, T. Nakayama and H. Kamimura: Solid State Commun. **66** (1988) 629.

[11] K.T.Park, K.Terakura, T.Oguchi, A.Yanase and M.Ikeda: J. Phys. Soc. Jpn. **57** (1988) 3445.

[12] K.Terakura, T.Oguchi, A.R.Williams and J.Kübler: Phys. Rev. **B30** (1984) 4734.

[13] K.Terakura, T.Oguchi, A.R.Williams and J.Kübler: Phys. Rev. Lett. **52** (1984) 1830.

[14] A.C.Wahl and G.Das: Modern Theoretical Chemistry, Vol.3, *Methods of Electronic Structure Theory*, ed. H.F.Schaefer (Plenum, 1977) p.51.

[15] S.Kato and K.Morokuma: Chem. Phys. Lett. **65** (1979) 19.

[16] M.Eto and H.Kamimura: Phys. Rev. Lett. **61** (1988) 2790.

[17] K.Ruedenberg and K.Sundberg: in *Quantum Science, Methods and Structure*, eds. J.C.Calais *et al.* (Plenum, 1977); B.Roos, P.R.Taylor and P.E.M.Siegbarn: Chem. Phys. **48** (1980) 157.

[18] N.F.Mott and E.A.Davis: *Electronic Processes in Non-Crystalline Materials* (Clarendon Press, Oxford, 1979) 2nd ed.

[19] *Proc. 19th Scottich Universities Summer School "The Metal Non-metal Transition in Disordered Systems,"* eds. L.R.Friedman and D.P.Tunstall (SUSSP Publications, Edinburgh, 1978).

[20] For a review, see *Anderson-Localization*, eds. Y.Nagaoka and H.Fukuyama (Springer, Berlin, 1982).

[21] For a review, also see Solid-State Electronics, Vol.28, No.112 (special issue) *Heavy Doping and the Metal-Insulator Transition in Semiconductors*, ed. P.T.Landsburg (1985).

[22] E.Abrahams, P.W.Anderson, D.C.Licciardello and T.V.Ramakrishnan: Phys. Rev. Lett. **42** (1979) 673.

[23] H.Kamimura: in Ref.[1], p.555.

[24] H.Kamimura: *Crystalline Semiconducting Materials and Devices*, eds. P.N.Butcher, N.H.March and M.P.Tosi (Plenum, 1986) p.305.



[25] E.Yamaguchi, H.Aoki and H.Kamimura: J. Phys. **C12** (1979) 4801.

[26] T.Takemori and H.Kamimura: Solid State Commun. 41 (1982) 885.

[27] Z.Gan and P.A.Lee: Phys. Rev. **B33** (1986) 3595.

[28] K.Andres, R.N.Bhatt, P.Goalwin, T.M.Rice and R.E.Walstedt: Phys. Rev. **B24** (1981) 244.

[29] R.N.Bhatt and P.A.Lee: Phys. Rev. Lett. **48** (1982) 344.

[30] M.P.Sarachik, A.Roy, M.Turner, M.Levy, D.He, L.L.Isaacs and R.N.Bhatt: Phys. Rev. **B34** (1986) 387.

[31] R.N.Bhatt: Physica Scripta. **T14** (1986) 7.

[32] T.Takemori and H.Kamimura: J. Phys. **C16** (1983) 5167.

[33] J.R.Marko, J.P.Harrison and J.D.Quirt: Phys. Rev. **B10** (1974) 2448.

[34] N.Kobayashi, S.Ikehata, S.Kobayashi and W.Sasaki: Solid State Commun. **24** (1977) 67.

[35] N.Kobayashi, S.Ikehata, S.Kobayashi and W.Sasaki: Solid State Commun. **32** (1979) 1147.

[36] W.Sasaki and J.Kinoshita: J. Phys. Soc. Jpn. **25** (1968) 1622.

[37] H.Ue and S.Maekawa: Phys. Rev. **B3** (1971) 4232.

[38] J.D.Quirt and J.R.Marko : Phys. Rev. **B5** (1972) 1716.

[39] J.D.Quirt and J.R.Marko : Phys. Rev. **B7** (1973) 3842.

[40] S.Ikehata, T.Ema, S.Kobayashi and W.Sasaki: J. Phys. Soc. Jpn. **50** (1981) 3655.

[41] A.L.Efros and B.I.Shklovskii: in Ref.[1], p.409 and related references cited therein.

[42] M.Pollak and M.Ortuno: in Ref.[1], p.287.

[43] T.F.Rosenbaum, R.F.Milligan, M.A.Paalamen, G.A.Thomas, R.N.Bhatt and W.Lin: Phys. Rev. **B27** (1983) 7509.

[44] G.A.Thomas, Y.Ootuka, S.Katsumoto, S.Kobayashi and W.Sasaki: Phys. Rev. **B25** (1982) 4288.

[45] Y.Nishio, K.Kajita, T.Iwata, and W.Sasaki: Proc. 18th Inter. Conf. Phys. Semicond. (Stockholm, Sweden 1986) 1257; Proc. 18th Int. Conf. Low Temp. Phys. (Kyoto, 1987) 691.

[46] Y.Gun, J Langlois and W.A.Goddard III: Science **239** (1988) 896.

[47] S.Yamamoto, K.Yamaguchi and K.Nasu: Phys. Rev. **B42** (1990) 266; K.Yamaguchi, Y.Takahara, T.Fueno and K.Nasu: Jpn. J. Appl. Phys. **26** (1987) L1362, L2037.

[48] Y.Asai: J. Phys. Soc. Jpn. **58** (1989) 3264.

[49] R.J.Cava, B.Batlogg, S.A.Sunshine, T.Siegrist, R.M.Fleming, K.Rabe, L.F.Schneemeyer, D.W.Murphy, R.B.van Dover, P.K.Gallagher, S.H.Glarum, S.Nakahara, R.C.Farrow, J.J.Krajewski, S.M.Zahurak, J.V.Waszczak, J.H.Marshall, P.Marsh, L.W.Rupp, Jr., W.F.Peck and E.A.Rietman: Physica **C153-155** (1988) 560.

[50] J.B.Boyce, F.Bridges, T.Claeson, T.H.Geballe, C.W.Chu and J.M.Tarascon: Phys. Rev. **B35** (1987) 7203.

[51] N.Shima, K.Shiraishi, T.Nakayama, A.Oshiyama and H.Kamimura: in *Proc. 1st Int. Conf. on Electronic Materials,* eds. T.Sugano, R.P.H.Chang, H.Kamimura, I.Hayashi and T.Kamiya (MRS, Pittsburgh 1988) p.51.

[52] E.Kaldis, P.Fischer, A.W.Hewat, E.A.Hewat, J.Karpinski and S.Rusiechi: Physica **C159** (1989) 668.

[53] C.Murayama, N.Mori, S.Yomo, H.Takagi, S.Uchida and Y.Tokuta: Nature **339** (1989) 293.

[54] R. J. Cava, A. Santoro, D. W. Johnson, Jr. and W. W. Rhodes: Phys. Rev. **B35** (1987) 6716. We use the lattice constants at 10 K reported there.



[55] F.Izumi, Y.Matsui, H.Takagi, S.Uchida, Y.Tokura and H.Asano: Physica **C158** (1989) 433.

[56] W.B.Pearson: *A Handbook of Lattice Spacings and Structures of Metals and Alloys,* (Pergamon, New York, 1958) p.1022.

[57] B.Roos, A.Veillard and G.Vinot: Theoret. Chim. Acta. **20** (1971) 1.

[58] T.H.Dunning Jr. and P.J.Hay: in Modern Theoretical Chemistry Vol.3, *Methods of Electronic Structure Theory,* ed. H.F.Schaefer III (Plenum, New York, 1977) p.1.

[59] S.Huzinaga, J.Andzelm, M.Klobukowski, E.Radzio-Andzelm, Y.Sakai and H.Tatewaki: Physical Sciences Data Vol.16, *Gaussian Basis Sets for Molecular Calculations,* eds. S.Huzinaga *et al.* (Elsevier, Amsterdam, 1984).

[60] F.C.Zhang and T.M.Rice: Phys. Rev. **B37** (1988) 3759.

[61] H.Kamimura: in *Progress in High Temperature Superconductivity Vol.14, Towards the Theoretical Understanding of High $T_c$ Superconductors,* eds. S.Lundqvist, E.Tosatti, M.P.Tosi and Y.Lu (World Scientific, Singapore) p.163.

[62] H.Kamimura, S.Matsuno and R.Saito: in the same book as in Ref.[5], p.8.

[63] H.Kamimura, S.Matsuno and K.Ishida: Physica. **C162-164** (1989) 781.

[64] K.A.Müller: in the same book as in Ref.[5], p.2 and related references therein.

[65] T.Fujita, Y.Aoki, Y.Maeno, J.Sakurai, H.Fukuba and H.Fujii: Jpn. J. Appl. Phys. **26** (1987) L368.

[66] J.B.Torrance, Y.Tokura, A.I.Nazzal, A.Bezinge, T.C.Huang and S.S.P.Parkin: Phys. Rev. Lett. **61** (1988) 1127.

[67] A.Fujimori: Phys. Rev. **B39** (1989) 793.

[68] K. B. Lyons, P. A. Fleury, J. P. Remeika, A. S. Cooper and T. J. Negran: Phys. Rev. **B37** (1988) 2353.

[69] S.Sugai: in the same book as in Ref.[5], p.207 and related references therein.

[70] S.Sugai, T.Kobayashi and J.Akimitsu: Phys. Rev. **B40** (1989) 2686.

[71] Y.Tokura, S.Koshihara, T.Arima, H.Takagi, S.Ishibashi, T.Ido and S.Uchida: Phys. Rev. **B41** (1990) 11657.

[72] R.E.Dietz, G.I.Parisot and A.E.Meixner: Phys. Rev. **B4** (1971) 2302.